GNSS Availability and Multipath Prediction in an Urban Environment

Thesis submitted to the Andhra University, Visakhapatnam in partial fulfillment of the requirement for the award of

Master of Technology in Remote Sensing and GIS

Submitted By:

Shikhar deep

Supervised By:

Mr. B.D. Bharath

Mr. S. Raghvendra

Indian Institute of Remote Sensing, ISRO,

Dept. of Space, Govt. of India Dehradun – 248001

Uttarakhand, India

August, 2013

Dedicated

To

My Nanaji & Naniji

Acknowledgements

It is my pleasure to acknowledge all those who have always inspired me to accomplish my goal. I wish to sincerely thank all those who were direct or indirect part of this work.

First and foremost, I would like to thank Almighty without whose blessings I could not have completed this work. I take this opportunity to express a deep sense of gratitude towards my guide Mr B.D Bharath, Scientist SE, URSD, IIRS for providing excellent guidance, encouragement and help all through the completion of this research work. I would like to express my deepest gratitude to my guide Mr. S. Raghvendra, Scientist SC, PRSD, IIRS for his astute technical advice and guidance throughout this work.

I thank Dr. Y.V.N Krishna Murthy, Director IIRS, for providing excellent research environment and infrastructure to pursue this research. I would also like to extend my deepest gratitude to Prof. B.S. Sokhi, Head URSD, IIRS for his constant support and providing critical inputs for making this project an invaluable learning experience. I am extremely grateful to Mrs. Shefali Agarwal, Head PRSD, IIRS & Course Director M.Tech for her timely encouragement and support which helped me for completion of this research work. Very special thanks to Andhra University, for providing this opportunity to undergo this M.Tech course at IIRS Dehradun. I also thank Dr Sadhana Jain & Dr Sandeep Maithani faculty URSD, IIRS for helping and guiding at various junctures during these two years.

A very special thanks to Col. K.K. Kakkar, for being my friend, teacher and guardian throughout these two years, inspiring and motivating at the time it was needed the most. I am thankful to Mr R.K. Bajpai (IFS) and Mr Prashant Dhanda (IFS) for not only being friends but also for motivation and guidance. I take this opportunity to thank all of my friends at IIRS particularly Upendra Bhai Patel, Deepak Upadhyay, Raghvendra Singh, Neha, Amit Singh, Vimal Pandey, Akansha, Shruti, Krithiga, Adesh sir, Ritika and Ragini for reminding me that there are many other important things in life.

I would also like to thank all the scientists at IIRS for their support during the course. My thanks are also to all the non-teaching staff of IIRS Campus, Hostel and Mess. Finally I pay my gratitude to my parents who brought me in this world. I am grateful to my maternal uncle who ensured that I reach this stage of fulfilment in my life.

(Shikhar Deep)

CERTIFICATE

This is to certify that the dissertation entitled **"GNSS Availability and Multipath Prediction in an Urban Environment "** is the original contribution of **Mr. Shikhar Deep** towards partial fulfillment of the of the requirement for the award of Master of Technology in Remote Sensing and GIS at Urban and Regional Studies Department, Indian Institute of Remote Sensing (IIRS), Dehradun.

The project contains original work carried out by him and he has duly acknowledged the sources of data and resources used.

.....	.....
(Mr. B.D. Bharath)	**(Mr. S. Raghvendra)**
Project Supervisor	Project Supervisor

.....	.....	.....
(Prof. B. S. Sokhi)	**(Dr. S. K. Saha)**	**(Dr.Y.V.N. Krishna Murthy)**
Head, URSD, IIRS	Group Director Earth Resources IIRS and System Studies Group and Dean (Academics), IIRS	Director, IIRS

Abstract

GNSS positioning in urban environment is difficult as the direct line of sight is obstructed. The signals received from reflection and diffraction from surrounding buildings aggravates the problem. Multipath is a major source of error in GNSS especially in an urban environment and cannot be even removed in differential mode. This research focuses on determining the correlation between the SNR and multipath errors. A regression model has been derived for finding the relation between SNR and elevation angle. Each satellite signal prediction has been successfully validated against the observed values taken from different building scenarios.

A software package has been developed for SNR prediction in urban environment incorporating reflection and diffraction from the surroundings. The other functions developed are for RINEX data processing, GPS field planning and addition of height from Cartosat 1 DEM to a 2D building shapefile. The height is provided from Cartosat 1 DEM to the 3D building model, an input for the multipath prediction model. To analyze the errors due to the resolution limit of the Cartosat 1 a 3D model was developed with Total Station.

The inverse relation of multipath errors with SNR has been derived. For the urban environment, the variation in GPS receiver antenna height and variation of surface materials in GPS positioning have been analyzed. The findings shows that increasing the antenna height decreases the multipath errors only when the SNR of the received signal is nearly equal or else increasing the antenna height may not exactly decrease the multipath residuals as then they follow the SNR inversely. The effect of variation of surface materials on accuracy is significant at low SNR only. The results show that for a wet surface the multipath residuals increases more than 100% at SNR less than 34dB, compared with the dry surface.

Multipath has been quantized using the linear phase combinations, code minus phase residuals and double differencing residuals. Stochastic and regression models have been derived to analyze the multipath residuals and relate them with SNR. The models relating SNR with pseudorange multipath are derived which could then be related to the positional accuracy. The importance of SNR being an important quality indicator has been proved.

Keywords: SNR, multipath error, multipath prediction model, antenna height variation, surface material variation, stochastic and regression models.

Table of Contents

List of Figures

List of Tables

Chapter 1: Introduction

1.1 Background

Today the GPS is an integral part of many systems ranging from communication to navigation. The functioning of these systems therefore is dependent on the positional accuracy given by the GPS. GPS is now being used in various urban and other information projects which require GPS measurements to be very precise. Taking GCPs for various small or large projects also requires having high positional GPS accuracy. GPS accuracy is mostly affected by the obstructions in any the form (buildings, trees and natural topography) which may lead to degradation of signal strength or complete signal blockage due to these obstructions. The position of any location cannot be computed if less than four satellites are visible or if satellite geometry at an instant is not proper we cannot get desired geometric dilution of precision (GDOP), which is generally a case in an urban environment. Real-time satellite availability prediction is very useful for mobile applications such as in-car navigation systems, personal navigations systems and location based services (LBS) (Taylor et al., 2007). In all such areas which require desired GPS accuracy and desired signal characteristics, preplanning for collection of GPS points can actually increase the efficiency if these values can be known in advance. GPS accuracy is a function of six major factors – geometry of satellites, ionospheric and tropospheric delays, satellite ephemeris (orbit), satellite clock error, receiver noise, and multipath (Beesley, 2002). In an urban environment, all of these factors except geometry of satellites and multipath affect GPS accuracy in a constant amount, so we need to deal with these two factors mainly. In this study the focus has been on the prediction of satellites with SNR in urban scenario, which finally would help the user for preplanning. The different urban scenarios have been discussed along with taking the different building materials. The thesis successfully concludes in quantifying the multipath and deriving its relation with Signal to Noise Ratio (SNR).

1.2 Motivation and Problem Statement

Reception of direct satellite signal is required for higher positioning precision. However, urban environment offers a challenge as various natural and built-up objects block the line of sight signals propagating from satellite to the end user and thus the deteriorated signals have an influence on the measurements, resulting error in position. The available signals reaching the user may be from indirect signal (reflection & diffraction) or a mix of both, which further degrades the accuracy. The use of multiple GNSS systems provides more satellites than the use of a single system, but not necessarily leads to better accuracies because most of the signals within such environments are affected by non-line of sight propagation. Thus in urban environment, multipath is the major error for GNSS positioning.

Not only the direct signals get blocked but also "poor geometry" (i.e. poor distribution of the available satellite signals over the sky) limits the precision. The use of GNSS will be very extensive

in various civil applications as (Huber et al., 2010) states some 3 billion satellite navigation receivers should be in service by 2020. Satirapod and Wang (2000) have compared SNR and satellite elevation, as quality indicators for GPS carrier phase observations, while (Kirchner and Becker, 2005) have shown that SNR data contain important information for deriving a reasonable weight of each individual phase observation. The additional observation type of SNR provides appropriate information to identify areas with degraded data quality due to multipath reflections. Ebner (2008) characterized the multipath effects on GNSS, especially GPS, in urban canyons, which discussed the degradation of the pseudorange estimates and the position error due to the multipath errors and then simulated with an urban canyon model. The demand for taking very precise GCPs for large scale mapping of urban areas is increasing and so the need of higher accuracy. With the increase in the number of users, GNSS today have become the core of all new intelligent traffic systems, requiring increasing accuracy in particular in dense urban areas. For this (Marais et al., 2010) proposed to build a new GNSS-based positioning algorithms adaptable to low cost receivers. The propagation of signals from satellite to GNSS receiver, ideally to be in line of sight but analyzing the signals tracked, it becomes apparent that more complex propagation modes must be considered as it's not always possible in case of urban environment, where sometimes signals reach after getting reflected or diffracted and sometimes they are blocked.

Signals are blocked at dense concentration of buildings surrounding a receiver. This effect is more where receivers are kept near ground surface. Urban environment, on the whole, consists of large surfaces, e.g. floors, roofs, windows and walls. The transmitted signals gets reflected from these smooth surfaces, thus reach the receiver via multiple paths. Similarly, the satellite signal gets bent at the building edges and reaches the receiver where LOS is blocked by the propagation mode called diffraction. Prediction of satellite availability is a strong asset in planning of routes, especially for safety of critical activities. Decision can be made in selection of one route over another based on lower GNSS signal degradation and higher satellite availability. At the time of this research, GPS and GLONASS are only fully operational GNSS. European GNSS (Galileo) is expected to reach full operating capability by 2019. It is important to establish the impact that these developments will have on positioning and navigation in the urban environment. The introduction of an improved civilian signal, referred to as L2C is intended to provide GPS civilian users with less susceptibility to multipath and more immunity to interference. A third frequency, L5, will be introduced for safety critical applications. The result of such developments will be that by around 2015, there will be somewhere in the region of 80 satellites for GNSS based positioning and navigation purposes (Bradbury, 2008).With the increasing number of satellites will increase the satellite availability and improve the geometry but positioning in deep urban canyons, these problems persist.

1.2.1 Issues in Static Positioning

The quality of results obtained from many surveying and location based applications is dependent upon accurate position determination using GNSS receivers. A lack of available signals, particularly in urban canyons, means that position determination in certain locations is impossible during certain periods throughout each day (Taylor et al., 2005). When most available signals originating from the

satellites are in the same vertical plane through sky, a poor DOP figure result, and it is the case in urban environment. Thus increment in satellite availability is unlikely to solve this problem. The signals received from propagation paths other than LOS, results in incorrect position determination that can be of the order of tens of meters (Yang et al., 2004) depending on the type of receiver. Therefore having the knowledge of the location and time where high/low quality satellite signals and its availability will be received, could be a strong input for decision making during GNSS surveys. Not only it will lead to short occupation time during survey but also gives user a choice of having better locations as user can plan the time of survey based upon signal quality and availability prediction.

1.2.2 Issues in Dynamic Positioning

Dynamic positioning also suffers the same problems as are with static positioning. For this purpose, mobile equipment with integrated GNSS receiver is used as in personal digital assistant (PDAs) with inbuilt navigation. Positioning in a mobile object, the magnitude of multipath error will be more as the range measurement will vary rapidly. Similarly, the satellite availability for dynamic positioning tends to change rapidly because of the relative motion between user and the surroundings. The applications using dynamic positioning operating in urban environment are generally used at ground level only where the interaction of satellite signals with the surroundings is highest. The use of inertial navigation system (INS) and map-matching resolves the difficulty of availability partially. Signal integrity is affected by frequent loss of lock in dynamic positioning.

1.3 Research questions and Research objectives

Research questions

- How to predict available satellites in a given urban environment, at a given point of time and at a given location?
- How a GPS signal quality gets affected in an urban environment?

Research objectives

- To predict signal reflection and diffraction from surfaces and edges.
- To predict the Multipath error along with SNR.
- To analyze satellite visibility at variable heights in an urban environment.

1.4 Outline of the thesis

Chapter one is the introduction which gives introduction about GNSS then describes about the background especially for the urban areas. The reasons for conducting this study are given as motivation further explaining about the problem statement. The research objectives and research questions are further elaborated.

Chapter two is the literature review where the GNSS, signal structure, observables and previous works done earlier having some kind of relevance with this study are discussed. The subtopics briefly explain the works done for modeling of multipath, stochastic models, taking the residuals by differencing and methods involving multipath mitigation. The chapter focuses on the concepts used and explains to reader the relation of multipath with other parameters.

Chapter third describes the study area where these values were validated, the data inputs taken for this study like GPS ephemeris, the softwares and the programming language used at various levels of the study. The reasons are provided for choosing the study area and brief description about the hardware used is discussed.

Chapter four describes the research methodology adopted for the work. Explaining every procedure followed, the chapter focuses on the multipath prediction model and the behavioral changes taking place due to it in the electrical properties of the signals.

The results are discussed in Chapter five. The program developed and its results are explained in the chapter. The chapter discusses various aspects of multipath with respect to urban environment and advantages of predicting satellites availability with their signal parameters. This chapter clearly brings out the benefits of predicting the multipath in various urban environments.

Chapter six concludes whole of the research with results achieving the objectives and describes the application of the research for the whole of urban environment. It also discusses the problems, answers the research questions and ends with the future work to be extended from this study. Based on the above results and conclusions, the recommendations are given which explain various aspects of using GNSS in urban areas.

Chapter 2: Literature Review & Theoretical Concepts

2.1 Theoretical concepts

This topic throws light on the on theoretical concepts used at various parts of the research.

2.1.1 Global Navigation Satellite System

A Global Navigation Satellite System (GNSS) system is based on a constellation of satellites that gives coverage over a wide region. In the last decade the GPS has found widespread use in all kind of applications. GPS is the first GNSS offering the accuracy needed for military and civil applications. It was designed by the U.S. Department of Defense initially proposed for satisfying an operational need of the United States military, the advent of the navigation signal timing and ranging global positioning system (NAVSTAR GPS) has also revolutionized the field of navigation, agriculture, forestry, natural resources applications, geodesy, surveying and scientific applications over the past two decades. In order to become independent about GPS system Russia came up with GLONASS while the European Union is developing Galileo as an equivalent of GPS. Other governments like Australia, China, Japan, and India also joined the league, if not in putting up their own full-edged navigation constellations, then at least to have satellite-based augmentation system (SBAS) or a regional navigation system. The requirements on precision, reliability and availability of the navigation system for these applications have become higher and higher.

2.1.2 GPS signal structure

The GPS signal uses bi-phase shift keying (BPSK) modulation. The rate of phase change is termed as the chip rate. The spectrum of the signal is spread spectrum and is represented by a sinc function. Usually CDMA signal is a spread-spectrum system. As the CDMA signals use the same carrier frequency, it increases the probability of interference. There are two types of GPS signals: the coarse/acquisition (C/A) code and precision (P) code. The actual P code is encrypted by a Y code, so it is often referred as the P(Y) code. Currently, the C/A code is used for civilian applications while the P(Y) code is reserved for military use. The GPS signals are transmitted on two different frequencies: L1 with 1575.42 MHz and L2 with 1227.6 MHz (Zheng, 2005).The wavelength of L1 being approximately 19cm and L2 having 24cm. The choice of GPS frequencies is a trade-off among ease of bandwidth allocation, smaller ionospheric delay errors, lesser space loss and availability of bandwidth for global transmission.

The L1 in-phase component is modulated by a P (precise) code and data bits, whereas quadrature-phase component is modulated by a C/A code and data bits. P and C/A codes are +/-1 ranging signals having chipping rates of 10.23 MHz and 1.023 MHz respectively, whereas navigation data bits are +/-

1 and have a frequency of 50 Hz. The wavelength of P code is 29.32m, ten times the resolution of the C/A code with wavelength 293.2m. Therefore, L1 satellite signal is then expressed as (Parkinson and Spilker, 1996).

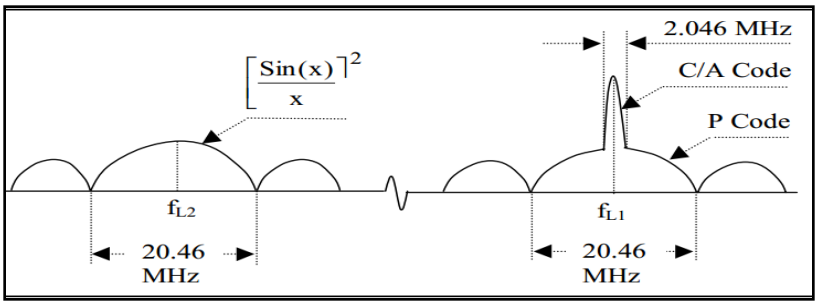

Figure 2.1 GPS signal power spectral density(Parkinson and Spilker, 1996)

$$f_{L1,i} = A_p XP_i(t)D_i(i)\cos(\omega_1 t + \varphi) + A_c XG_i(t)D_i(t)\sin(\omega_1 t + \gamma_1) \quad (2.1)$$

where,

i	is the satellite index
A_p, A_c	are the in-phase and quadrature signal amplitudes respectively (volt, volt)
XP, XG	are the P and C/A code respectively
D	is the navigation data bit
ω_1	is the L1 centre frequency(rad/s), and
γ_1	is the small phase noise and oscillator drift component(rad).

The L2 signal is biphase modulated by either a P or a C/A code as selected by the ground command and the same data bits as in L1. Therefore the L2 satellite signal is

$$f_{L2,i(t)=} B_P XP_i(t)D_i\cos(\omega_2 t + \gamma_2) \quad (2.2)$$

where

B_P	is the L2 signal amplitude(volt)
ω_2	is the L2 centre frequency(rad/s)
γ_2	is the phase noise(rad)

The P code is replaced by the Y code when anti-spoofing (AS) is activated. The P Code is bi-phase modulated at 10.23 MHz and the main lobe of the spectrum is 20.46 MHz wide from null-to-null. The code is generated from two pseudorandom noise (PRN) codes with the same chip rate of 10.23 MHz. The C/A Code is a bi-phase modulated signal with a chip rate of 1.023 MHz with a null to-null bandwidth of the main lobe of the signal spectrum of 2.046 MHz. However, the transmission bandwidth of the GPS signal at the L1 frequency is approximately 20 MHz to accommodate the bandwidth needed for the P code signal. Therefore, in addition to the main lobe of the C/A code signal, several side lobes of the signal are also transmitted in this bandwidth.

2.1.3 GPS observables

The GNSS signals after getting processed yield basically two observables namely code and phase solutions which are most important observables.

Code observations: Also called pseudorange observation is not very precise measure of the receiver-satellite distance. Time difference between signal transmission from satellite and reception at receiver gives the following basic code observation equation (Verhagen, 2005).

$$p_{r,j}^{s}(t) = c[t_r(t) - t^s(t - \tau_r^s)] + e_{r,j}^{s}(t) \quad (2.3)$$

with:

$p_{r,j}^{s}(t)$	code observation at receiver r from satellite s on frequency *j*[m]
t	time of observation in GPS time[s]
c	velocity of light in vacuum [m/s]
t_r	reception time at receiver *r*[s]
t^s	transmission time from satellite *s*[s]
τ	signal travel time[s]
e	code measurement error

As the satellite clock time and the receiver clock time are not same as GPS time, therefore respective clock errors dt_r and dt^s are taken.

$$t_r(t) = t + dt_r(t) \quad (2.4)$$

$$t^s(t - \tau_r^s) = t - \tau_{r,j}^{s} + dt^s(t - \tau_r^s) \quad (2.5)$$

Inserting equations (1.4) and (1.5) in equation (1.3) gives:

$$p_{r,j}^{s}(t) = c\tau_{r,j}^{s} + c[dt_r(t) - dt^s(t - \tau_r^s)] + e_{r,j}^{s}(t) \quad (2.6)$$

In order to determine the geometric distance between the satellite and receiver, the signal travel time $\tau_{r,j}^{s}$ needs to be corrected for instrumental, atmospheric and multipath errors.

$$\tau_{r,j}^{s} = \delta\tau_{r,j}^{s} + d_{r,j} + d_j^s \quad (2.7)$$

$$\delta\tau_{r,j}^{s} = \frac{1}{c}\left[\rho_r^s + da_{r,j}^{s} + d_j^s\right] \quad (2.8)$$

with:

$\delta\tau$	signal travel time from satellite antenna to receiver antenna[s]
dr	instrumental code delay in receiver[s]
ds	instrumental code delay in satellite[s]
ρ	geometric distance between satellite and receiver[m]
da	atmospheric code error[m]
dm	code multipath error[m]

inserting above equations (2.7) and (2.8) in the equation (2.6) gives the following

$$p_{r,j}^{s}(t) = \rho_r^s(t, t - \tau_r^s) + da_{r,j}^{s}(t) + dm_{r,j}^{s}(t) + c\left[dt_r(t) - dt^s(t - \tau_r^s) + d_{r,j}(t) + d_j^s(t - \tau_r^s)\right] + e_{r,j}^{s}(t) \quad (2.9)$$

The atmospheric, multipath and instrumental errors are different for code and phase measurements.

Phase observations: It is very precise measure of the geometric distance between a satellite and receiver. It is the difference between phase generated at receiver and phase generated at satellite of the carrier signal during transmission. The measure of total number of integral full cycles is unknown and is termed as carrier phase ambiguity. The following is the carrier phase observation equation.

$$\varphi_{r,j}^{s}(t) = \varphi_{r,j}^{s}(t - \tau_r^s) + N_{r,j}^{s} + \varepsilon_{r,j}^{s}(t) \quad (2.10)$$

with:

φ	carrier phase observation [cycles]
N	integer carrier phase ambiguity

ε phase measurement error

The phases on the right hand side are equal to:

$$\varphi_{r,j}(t) = f_j t_r(t) + \varphi_{r,j}(t_0) = f_j\left(t + dt_r(t)\right) + \varphi_{r,j}(t_0) \quad (2.11)$$

$$\varphi_j^s(t) = f_j t^s(t - \tau_r^s) + \varphi_j^s(t_0) = f_j\left(t - \tau_{r,j}^s + dt^s(t - \tau_r^s)\right) + \varphi_j^s(t_0) \quad (2.12)$$

f nominal carrier frequency[s^{-1}]

$\varphi_r(t_0)$ initial phase in receiver at zero time[cycles]

$\varphi^s(t_0)$ initial phase in satellite at zero time[cycles]

The carrier phase observation equation becomes:

$$\varphi_{r,j}^s(t) = f_j\left[\tau_{r,j}^s + dt_r(t) - dt^s(t - \tau_r^s)\right] + \left[\varphi_{r,j}(t_0) - \varphi_j^s(t_0)\right] + N_{r,j}^s + \varepsilon_{r,j}^s(t) \quad (2.13)$$

This equation must be transformed to obtain units of meters and is therefore multiplied with the nominal wavelength of the carrier signal: $\emptyset_j = \lambda_j \varphi_j$

with $\lambda_j = \frac{c}{f_j}$

The carrier signal travel time is expanded similarly as in equations 2.7 and 2.8. This results in the following observation equation:

$$\varphi_{r,j}^s(t) = \rho_r^s(t, t - \tau_r^s) + \delta a_{r,j}^s(t) + \delta m_{r,j}^s(t) + c\left[dt_r(t) - dt^s(t - \tau_r^s) + \delta_{r,j}(t) + \delta_j^s(t - \tau_r^s)\right] + \left[\phi_{r,j}(t_0) + \phi_j^s(t_0)\right] + \lambda_j N_{r,j}^s + \varepsilon_{r,j}^s(t) \quad (2.14)$$

Generally the error induced by multipath on the code measurements varies between 1 and 5 meters and the effect on the phase measurements is of 1-5 cm (Verhagen, 2005).

2.1.4 DOP

DOP completely determines the geometry of the satellites. It is an important factor in deciding positional accuracy as it relates to ranging accuracy. The relation of rms positional error to rms of pseudorange error is as follows (Parkinson and Spilker, 1996)

$$\sigma_{\text{Positional error}} = \text{DOP} * \sigma_{\text{pseudorange}} \quad (2.15)$$

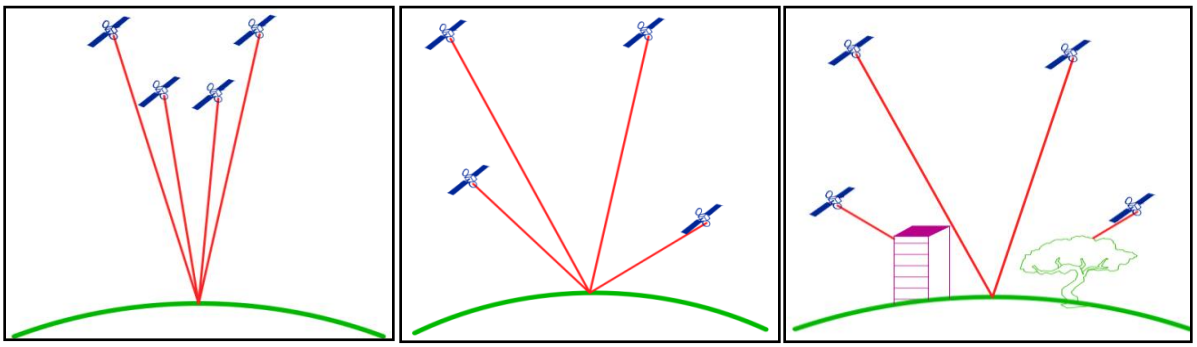

(a) Poor GDOP (b) Good GDOP (c) Good GDOP Poor visibility

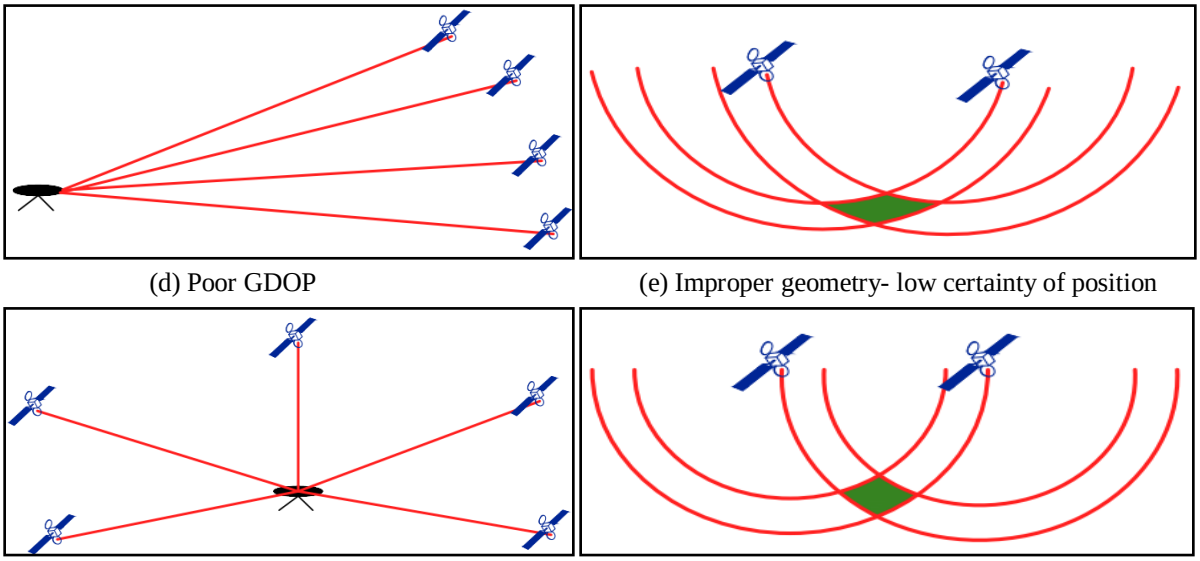

(d) Poor GDOP (e) Improper geometry- low certainty of position

(f) Good GDOP (g) Proper geometry - high certainty of position

Figure 2.2 Satellite Geometries showing DOP

Whenever the satellite geometry is such that all the satellites are close together or not spread uniformly in the sky, the overlap between them is much larger, increasing more uncertainty of the GPS location to be than the condition when visible satellites are spread properly are far apart. The Figure 2.2 (e) and Figure 2.2 (g) demonstrated how the satellite geometry decides the uncertainty in the position. As given by (Dana, 1997) **,** the spatial geometry for GDOP values is depicted in all the figures. The above figures explain clearly how satellite geometry affects the accuracy and not just having more than more four satellites visible will be enough but atleast four well spread and well distant satellites are required for the purpose.

2.1.5 IGS Ephemeris

International GNSS Service (IGS) was previously called International GPS service. It's the association of more than 200 voluntary organisations which consists of data centers, tracking stations and analysis centers working to generate precise GPS & GLONASS products. The data products are used for education, research and other multidisciplinary applications. It is the global network of permanent stations generating, tracking and providing raw orbit data. The data centers collect the raw data, convert to a common format then transmit to global data center, archived from where the users can access for various products. The products that are generated are global ionospheric maps, GPS satellite, IGS tracking station clock information, Earth rotation parameters, GLONASS satellite ephemerides, GPS satellite ephemerides, Zenith tropospheric path delay estimates, IGS tracking station coordinates and velocities (http://igscb.jpl.nasa.gov/overview/viewindex.html).

There are three types of solutions that are computed of GPS ephemeris, clock and earth orientation. The first solution is called final, these combinations are available after 12days while the second combination called rapid are available after 17 hours. The third combinations are called the ultrarapid

product, which are released four times in a day and are named according to midpoint time in the file: 00, 06, 12, and 18 UT. They have orbits of 48hours of which first half are computed ones while the rest are predicted ones.

2.1.6 RINEX

Receiver Independent Exchange Format (RINEX) was developed by the Astronomical Institute of the University of Berne for the purpose of the easy exchange of the GPS. It was used for European GPS campaign EUREF 89. The main points that were taken into account during its development were; mostly the processing softwares for GPS data work with well-defined set of observables namely, the carrier-phase measurement at one or both carriers, the pseudorange (code) measurement and the observation time. Most of the information is usually stored in the receiver itself, some additional station-related information like station name, antenna height etc. is needed. The general format has of 6 types of ASCII files namely Observation Data File, Navigation Message File, Meteorological Data File, GLONASS Navigation Message File, GEO Navigation Message File and Satellite and Receiver Clock Date File (Gurtner, 2007). RINEX is a standard format and helps in post processing to get more accurate solution. It works very well when some other parameters like atmospheric conditions are to be calculated or modeled during post processing. The final result of the receiver is generally its position.

2.1.7 Electromagnetic Properties of the GPS Signal

Electromagnetic (EM) waves are formed when an electrical field is coupled with a magnetic field. During the wave propagation, the time-varying magnetic and time-varying electric field generates each other and propagates through the empty space at the velocity of light. It is depicted in Figure 2.3 (Ray, 2000a) that GPS signal is a transverse electromagnetic (TEM) wave, implying electric (E) and magnetic (H) field are perpendicular to the direction of propagation. The tip of time-varying electric field component decides the polarization.

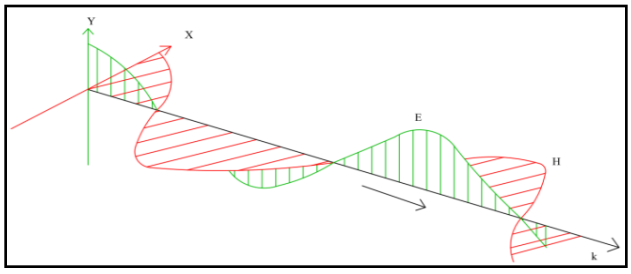

Figure 2.3 Electromagnetic wave progation

If the direction of the electric field remains unchanged with time, the wave is linearly polarized. If the electric field vector rotates as a function of time, the tip defines its polarization to be either elliptical or circular. Various polarizations are shown in Figure 2.4 (Ray, 2000a).The GPS signal is a right-handed circular polarized (RHCP) TEM wave.

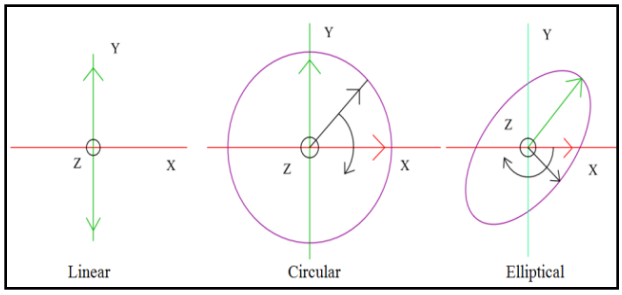

Figure 2.4 Linear,Circular and Elliptical polarization

Right-handed means, "that the rotation from E to H is in the direction of a right-hand-threaded screw if seen along the direction of propagation" (Kraus and Carver, 1973).

2.1.8 Reflection of Electromagnetic wave

The signal gets reflected and scattered of the surface into two components namely specular and diffuse. Reflection changes magnitude, polarization, direction and phase of the signal. When the signal is almost perpendicular to the surface, maximum change in polarization takes places turning into left-handed circular polarization (LHCP). When reflection is from smooth surface specular reflection occurs while the diffuse occurs reflecting from rough surface. Surface roughness and smoothness have been quantified by Rayleigh with the following criterion. The surface is said to be smooth if

$$\Delta h < \frac{\lambda}{8sin\theta} \tag{2.16}$$

Δh is the mean height of the irregularities within the First Fresnel ellipse, λ wavelength of the signal and θ elevation angle of the signal (rad). Further details on reflection theory and its effects on polarization can be found in (Hannah, 2001) and (Kraus and Carver, 1973).

2.1.9 Electrical properties of building materials

The two main electrical properties of the construction materials affecting the reflection coefficients are relative permittivity and conductivity. The materials concrete, glass and coal-tar being most widely used in urban environment are discussed here. (O'Shaughnessy, 2012) defined the permittivity and conductivity as following:

Permittivity (ε) : Permittivity is the property of a material relating the electric flux density to the electric field. Its unit is Farads per meter (F/m). The relative permittivity ε_r is ratio of permittivity to permittivity to vacuum permittivityε_o.

$$\varepsilon_r = \frac{\varepsilon}{\varepsilon_0} \tag{2.17}$$

It is another term used for dielectric constant, indicating the strength of the polarizing medium. The values of relative permittivity for concrete, glass and coal-tar are 3, 6 and 2.5 (Wilson, 2002).

Conductivity (σ): is the property of a material measuring the ratio between its current density and electrical field density. Its unit is Siemens per meter (S/m). The values of conductivity for concrete, glass and coal-tar are 2*10-5 ,10−11 and 10-14 S/m (Bouchiat et al., 1999).

The complex relative permittivity is related to relative permittivity and conductivity by the following relation (Zajícek and Vrba, 2010):

$$\varepsilon = \varepsilon_r - j\frac{\sigma}{\omega\varepsilon_0} \tag{2.18}$$

2.1.9.1 Linear Reflection Coefficient

Multipath is not only affected by the geometry of the surroundings and electrical properties but also of the electrical properties. The nature of reflected signals is explained by the Fresnel equations for specular reflection. The Linear Reflection Coefficients for vertical (Γ_V) and horizontal (Γ_H) polarizations plotted in Figure 2.5 are (Fresnel, 2001):

$$\Gamma_H = \frac{\sin\theta - \sqrt{\varepsilon - \cos^2\theta}}{\sin\theta + \sqrt{\varepsilon - \cos^2\theta}} \tag{2.19}$$

$$\Gamma_V = \frac{\varepsilon\sin\theta - \sqrt{\varepsilon - \cos^2\theta}}{\varepsilon\sin\theta + \sqrt{\varepsilon - \cos^2\theta}} \tag{2.20}$$

With the above equations the linear reflection coefficient can be easily calculated for a given set of grazing angle (θ), dielectric constant, frequency and conductivity for a particular surface using equation 2.18. The reflection coefficients of concrete and the coal-tar represent more or less same reflection coefficients in both the polarisations. The reflection coefficient of glass is much higher than rest of the two. The general trend is horizontal polarisation decreases uniformly with phase shift of 180 degree while the vertical polarisation first decreases and reaches to lowest point (the angle corresponding to it is Brewster' angle) then increases, thus the phase shift is 180 for angles less than Brewster's and greater than this the phase shift is zero. The resulting polarisation will depend upon these two and their phases.

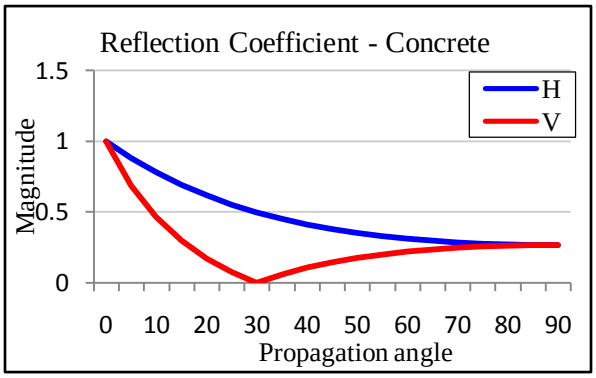

(a) Concrete

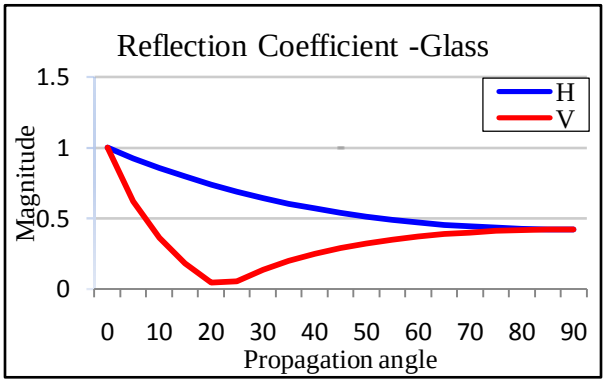

(b) Glass

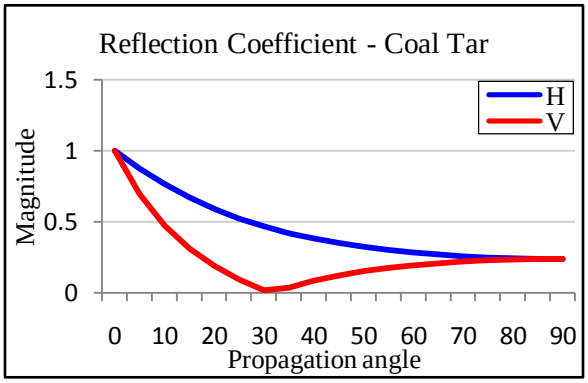

(c) Coal-Tar

Figure 2.5 Linear reflection coefficients

For the angles less than Brewster's angle the reflected GPS signal is RHEP while greater than this the polarisation of the reflected signal reaches to that of LHEP. For the purpose of modeling the GPS RHCP L1 signal circular reflection coefficients is used.

2.1.9.2 Circular Reflection Coefficient

The use of co-polarisation (Γ_o) and cross-polarisation (Γ_x) helps in modeling of GPS RHCP L1 signal.

$$\Gamma_o = \frac{\Gamma_H + \Gamma_V}{2} \tag{2.21}$$

$$\Gamma_x = \frac{\Gamma_H - \Gamma_V}{2} \tag{2.22}$$

The magnitudes of the co-polarisation and cross -polarisation are plotted for the concrete, glass and coal-tar surface with equations 2.21 and 2.22. The plots show that at Brewster angle the co-polarisation and cross-polarisation are equal and thus the polarisation will be circular. When they are different polarisation will be elliptical. These graphs also confirm the above thing that reflected signal is right hand elliptically polarized (RHEP) before the Brewster angle and increasing the propagation angle above it the signal becomes highly right hand elliptically polarized (LHEP) at 90 degrees.

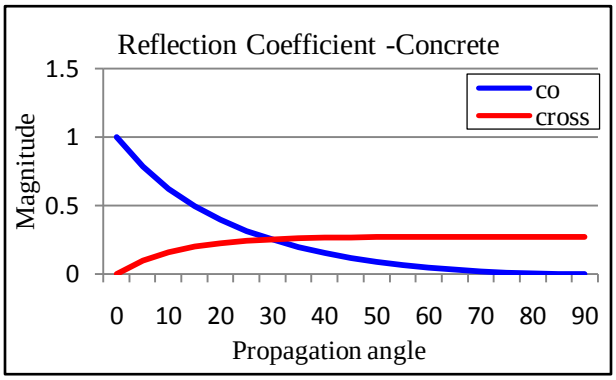

(a) Concrete

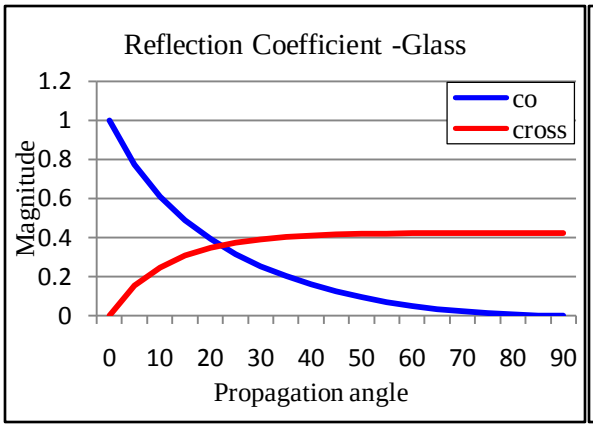

(b) Glass

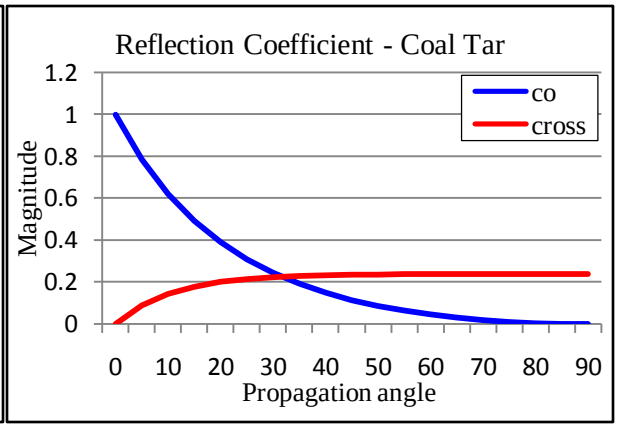

(c) Coal-Tar

Figure 2.6 Circular reflection coefficients

2.1.10 Diffraction

Whenever the electromagnetic wave encounters the edge of an obstacle, then the phenomenon of bending of rays taking place is called diffraction. It leads to weakening of the signal as the signal travels a longer distance with that of the direct resulting in the causing the positioning error. Generally SNR is correlated with diffraction contaminated signals (Richter and Euler, 2001). Here a

single knife-edge diffraction model is used for modeling the diffraction loss as per the International Telecommunication Union Radio Communication standard. It caters both LOS and NLOS cases.

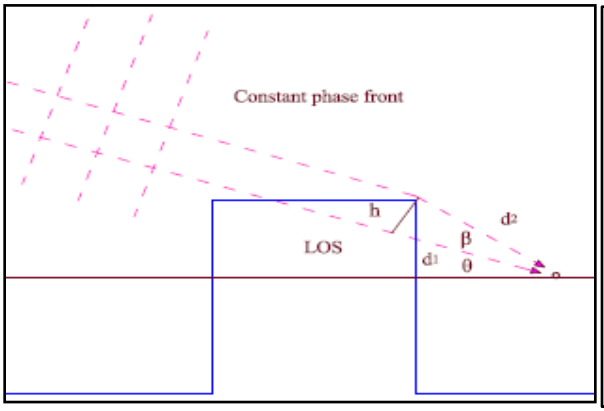

Figure 2.7 Diffraction at a building

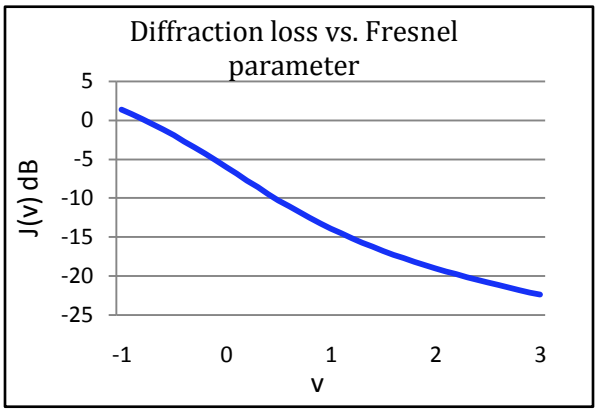

Figure 2.8 Diffraction gain v/s Fresnel Parameter

In the Figure 2.7, h is the perpendicular distance from the LOS, d^1 is the distance of the obstruction from that of the satellite, d^2 is the distance of the obstruction from the receiver and v is the Fresnel parameter.

$$v = h\sqrt{\frac{2}{\lambda d^2}} \tag{2.23}$$

For the condition v greater than -0.7 the diffraction gain (Li et al., 2008) is given by following equation. The variation between the diffraction loss and the Fresnel Parameter is shown in Figure 2.8.

$$J(v) = 6.9 + 20\log\left(\sqrt{(v-0.1)^2+1} + v - 0.1\right) dB \tag{2.24}$$

2.1.11 Antenna gain pattern

GPS antenna plays an important role in the reception of the signals. The various parameters that affect the signal quality are LHCP rejection ratio, phase stability, repeatability, gain vs. azimuth, gain vs. elevation, size, profile and surroundings (Dierendonck et al., 1996). The antenna gain decides the attenuation on the incoming signal. The purpose is to have gain distributed uniformly above certain elevation for all satellites while rejecting the ones with multipath signals. Thus the antenna gain pattern is such that the low gain is for low elevation satellites (generally multipath signals) and high gain for high elevation angles. GPS signal being the RHCP so the antenna must have high LHCP rejection ratio so as to reject the multipath signals. The calculations done are for single reflection from the boundary. As the GPS signal is RHCP the antennas are designed to have RHCP only rejecting the LHCP part as it contains multipath signals defined by LHCP rejection ratio. Here also for modeling the complete reflection coefficient of RHCP GPS signal boundary conditions for both the polarisations would be required. To simplify it, effective CP reflection coefficient for RHCP signal is calculated making taking LHCP rejection ratio factor in cross-polarised component (Hannah, 2001).

$$\Gamma_R = \left(\Gamma_o + 10^{\frac{-K}{20}}\Gamma_x\right)e^{-j\pi} \quad (2.25)$$

Similarly for the LHCP signal the effective LHCP reflection coefficient incorporating the LHCP rejection ratio is

$$\Gamma_L = \left(10^{\frac{-K}{20}}\Gamma_o + \Gamma_x\right)e^{-j\pi} \quad (2.26)$$

The LHCP rejection ratio is represented by K in dB for the GPS antenna and is 20 for Trimble Zephyr geodetic model 2.

2.1.12 SNR vs. Elevation angle

SNR determines the quality of the signal as it the ratio of the power of the GPS carrier signal to the noise power. SNR is affected by factors external and internal to GPS receiver. External factors include space loss, transmitted power, multipath and atmospheric losses while internal ones are tracking loop design and antenna gain pattern. The SNR is stored in all the GNSS receivers, but there is no uniform method of calculating it. Therefore the values may differ from one manufacture to other. The noise level in a geodetic GPS receiver is almost constant, so the SNR is directly proportional to the GPS received signal strength. (Bilich et al., 2004), (Collins and Langley, 1999) have shown that variation pattern of SNR and elevation are same. Here also, we found a polynomial relation between the SNR and elevation angle as given in equation no 5.1.

2.1.13 Linear phase combinations

We get the GPS observables from the RINEX. The pseudorange multipath can be analyzed using the linear phase combinations. It eliminates the clock and atmospheric errors. It is derived by the following equations derives (Langley et al., 1998), (Estey and Meertens, 1999), (Ge et al., 2002):

$$MP_1 = P1 - 4.0915\phi_1 + 3.0915\phi_2 + \left[4.0915\left(\lambda_1 N_1 + MP_{\phi 1}\right) - 3.0915\left(\lambda_2 N_2 + MP_{\phi 2}\right)\right] \quad (2.27)$$

$$MP_2 = P2 - 5.0915\phi_1 + 4.0915\phi_2 + \left[5.0915\left(\lambda_1 N_1 + MP_{\phi 1}\right) - 4.0915\left(\lambda_2 N_2 + MP_{\phi 2}\right)\right] \quad (2.28)$$

Carrier phase multipath is negligible so $MP_{\phi 1}, MP_{\phi 2}$ are ignored. The biases in the remaining terms are almost constant provided there is no cycle slip, thus with averaging can be removed leaving the pseudorange multipath residuals along with receiver noise.

2.1.14 Code-minus-Carrier (phase)

It determines the code noise and the terms that are removed in this are tropospheric delay, clock errors (satellite and receiver) and geometric range. The phase noise and multipath are not taken assuming them to be negligible comparing with code phase and multipath (Bakker et al., 2009). It is done here by removing low-order polynomial fit from code minus phase data which removes constant

ambiguities, hardware delays, low frequency ionospheric delay and low frequency multipath leaving the high frequency terms of ionospheric delay, code multipath and noise.

2.1.15 Stochastic Model

Modeling in GPS processing has always been an important part, which help in various aspects of precision observations. SNR has also been mainly used in multipath mitigation models. With the recent trend it is now being used in stochastic models, the stochastic model relates the statistics of the GPS observables and is used in high precision applications. The importance of stochastic models has been focused in many researches (Satirapod and Wang, 2000). The advantage of using stochastic models is that it can incorporate some of the unmodeled biases and thus improve the accuracy. Parkinson and Spilker (1996) relate the RMS phase noise and the SNR as:

$$\sigma^2 \cong \frac{1}{SNR_L} \qquad 2.29$$

In this study the one such model is used and has been modified for the observations from Trimble GNSS R7 which is discussed in results. The stochastic model relates the error due to code multipath and noise with that of the SNR. Thus a strong relation between the two can be made to comment on the effect of multipath on SNR, which further can be related to positional accuracy using the relation given by equation 2.15.

2.1.16 GPS observation differences

Differencing of the GPS observables proves to be an effective technique as the common errors are eliminated (Zinas, 2011).

2.1.16.1 Single Difference Observable

We know from equation 2.14 the deterministic model for the carrier phase in meters is given as:

$$\varphi_r^s(t) = \rho_r^s(t, t-\tau_r^s) + \delta a_r^s(t) + \delta m_r^s(t) + c[dt_r(t) - dt^s(t-\tau_r^s) + \delta_r(t) + \delta^s(t-\tau_r^s)] + [\phi_r(t_0) + \emptyset^s(t_0)] + \lambda_j N_r^s + \varepsilon_r^s(t) \qquad \text{from (2.14)}$$

Single differencing observables (φ_{br}^1) are formed by taking the difference of the phase observable, of the same signal of a particular satellite received by two GPS receivers. The receiver clock errors of the receiver are different but the satellite clock errors are same and get cancelled in single differencing. Here the subscripts showing b for base and r for rover.

$$\varphi_{br}^1 = \varphi_b^1 - \varphi_r^1 = \rho_b^1(t, t-\tau_b^1) - \rho_r^1(t, t-\tau_r^1) + \delta a_b^1(t) - \delta a_r^1(t) + \delta m_b^1(t) - \delta m_r^1(t) + cdt_b(t) - cdt_r(t) + c\delta_b(t) - c\delta_r(t) + \lambda N_b^1 - \lambda N_r^1 + \varepsilon_b^1(t) - \varepsilon_r^1(t) \qquad (2.30)$$

Taking the difference of the two satellites received by same satellite removes the receiver clock errors and clock bias. $\varphi_b^{12} = \varphi_b^1 - \varphi_b^2$

$$\varphi_b^1 - \varphi_b^2 = \rho_b^1(t, t-\tau_b^1) - \rho_b^2(t, t-\tau_b^2) + \delta a_b^1(t) - \delta a_b^2(t) + \delta m_b^1(t) - \delta m_b^2(t) + cdt_b^1(t) - cdt_b^2(t) + c\delta_b^1(t) - c\delta_b^2(t) + \lambda N_b^1 - \lambda N_b^2 + \varepsilon_b^1(t) - \varepsilon_b^2(t) \quad (2.31)$$

2.1.16.2 Double Difference Observable

Taking the difference between the two single differences a double difference observable is formed. The error sources which are receiver independent affecting the carrier phase measurements are multipath error, atmospheric errors (ionospheric and tropospheric) and measurement noises.

$$\varphi_{br}^{12} = \varphi_b^{12} - \varphi_r^{12}$$
$$= \rho_b^{12} - \rho_r^{12} + \delta m_b^{12} - \delta m_r^{12} + \lambda N_b^{12} - \lambda N_b^{12} + \delta a_b^{12}(t) - \delta a_b^{12}(t) + \varepsilon_b^{12}(t) - \varepsilon_b^{12}(t) \quad (2.32)$$

Double differencing effectively cancels out satellite clock offsets and clock biases as its differencing involves two satellites and two receivers. Double differencing results ambiguity parameter to be integer as it involves elimination of clock and hardware delays which create the non-integral terms.

2.1.16.3Triple Difference Observable

Taking the difference of two double difference residuals a triple difference observable is formed. The terms which are constant between the epochs are eliminated. It also leads to elimination of double difference ambiguities, thus can be used for detection and correction of cycle slips.

$$\varphi_{br}^{12}(t+\Delta t) - \varphi_{br}^{12}(t)$$
$$= \rho_{br}^{12}(t+\Delta t) - \rho_{br}^{12}(t) + \delta m_b^{12} - \delta m_r^{12} + \delta a_{br}^{12}(t+\Delta t) - \delta a_{br}^{12}(t) + \varepsilon_{br}^{12}(t+\Delta t) - \varepsilon_{br}^{12}(t) \quad (2.33)$$

2.2 Literature review

The literature reviewed for this research under different sub headings of multipath is discussed in following sections.

2.2.1 Multipath modeling

A method was proposed by (Scappuzzo, 1997), for the estimation of GPS multipath phase error manipulating the SNR of the received GPS signal itself to perform estimation and found in most of the cases that a broad-band coherence function between the observed phase error and the estimated multipath phase error in presence of strong multipath. (Ray et al., 1999), (Alber et al., 2000) developed a multipath simulation model and described wherein the multipath parameters can be varied and their influences are observed. The parameters included are the reflection coefficient, the antenna to reflector distance, the azimuth and elevation of the reflected signal the existence of multiple reflectors and satellite dynamics. Multipath was analyzed taking differences. Single-path phase delays were obtained from GPS doubles differences, an application of which was sensing of

atmospheric water vapor remotely by (Alber et al., 2000). Hannah (2001) united the existing theory of radio frequency propagation for the GPS L1 signal into a coherent treatment of GPS propagation in the terrestrial environment and described the design and development of a new parabolic equation based propagation model for analysis of GPS multipath propagation behavior. Similar work on Electromagnetic Modeling for GPS carrier phase multipath signals was presented by (Fan and Ding, 2006) which showed that static multipath modeling experiments reduced carrier phase errors up to 35% and 3D positioning errors up to 25%.

The problem of GPS signal delay estimation in a multipath environment was addressed (Soubielle et al., 2002) and maximum-likelihood estimator (MLE) was studied based on a signal model including the parametric contribution of reflected components. (Byun et al., 2002) developed a ray tracing GPS signal multipath simulator which takes into account the signal reflection and diffraction from surrounding objects. By properly modeling the environment around the antenna and the GPS receiver's tracking loop, the simulator can assess the GPS signal multipath error. Later (Fantino et al., 2004) worked on a modified version of the conventional tracking scheme with the aim of monitoring the quality of the measurements at the signal processing level particularly considering the problem of multipath while (Kirchner and Becker, 2005) presented a SNR weighting strategy to evaluated the positive impact to the processing. To improve the quality of GPS static phase data (Betaille et al., 2006) came up with a new method showing improvement between 10% and 20% depending on the length of the additional path travelled by the reflected signal. (Bilich et al., 2007) have established lot of principles linking dual-frequency SNR data, pseudorange multipath, phase multipath and used the application of SNR measurements to screen and improve carrier phase data for subsequent positioning analysis. Further they presented observations of SNR data from a continuously operating GPS receiver, which show strong evidence of ground and monument multipath. A tool called power spectral mapping was then presented by (Bilich and Larson, 2007) that visually represents the multipath environment of a GPS site, using the spectral content of SNR time series to determine which satellites contribute significant multipath error and at what frequencies. The simulated environment plays an important role in prediction of satellite availability and modeling of the reflected signals and thus analysis of multipath effects on pseudorange (Bradbury, 2008), (Ebner, 2008), (Schubert et al., 2008), (Suh et al.) and (Mekik and Can, 2010). Even-Tzur and Shaked (2008) attempted to examine the effects of the antenna height on pseudorange multipath in a variety of GPS antennas, and compared the multipath mitigation capabilities of different antennas, set up at different heights. (Marais et al., 2005) proposed a new tool to predict the availability of satellite constellation from the point of view of the land transportation. In recent past several works have been published examining multipath effects on pseudo-ranges and Doppler measurement especially in urban areas by (Ben-Moshe et al., 2011). The work has been extended to monitor deformation in any built up structure or mountain like (Esteban Vázquez B and Grejner-Brzeziska, 2012) conducted at Trans Antarctic Mountain Deformation network. Contemporary researches have focused in development of new algorithms based on 3D maps so as to reduce the complexity by (Obst et al., 2012).

The improvement in the hardwares, especially antenna, have also been worked so as to remove multipath errors as suggested by (Park et al., 2002). The focus has been extended to the development of softwares so that tracking errors become multipath invariant. The techniques have been extended (Ge et al., 2002) to adaptive filter using the least-mean-square algorithm for detection of multipath. The new expressions for the multipath-induced pseudorange error and variance due to multipath onto the time of arrival estimate are obtained by (Fante and Vaccaro, 2003).

2.2.2 Stochastic modeling

The main issues in handling the multipath are modeling of it, assigning correct stochastic model and with its results calibrating the GPS systems (Lau and Cross, 2007). Kim and Langley first introduced the multipath divergence problem then proposed a new procedure to overcome the multipath problem in the previous approaches. The stochastic models have improved the positional accuracy during post processing and have used an extended Kalman filter to reduce the effects of errors (Iyiade, 2005). It has been shown by (Wieser et al., 2005) that SIGMA-ε can correctly model more than 99% of the L1 pseudo-range errors in benign environment while (Cederholm, 2010) investigated statistical properties of L1 carrier phase observations from four low-cost GPS receivers . Single and double differences remove most of the errors and the residuals are left with the influence of multipath on them and thus multipath can be correlated with the residuals taking differences and has been studied in various forms or combinations (Serrano et al., 2005), (García et al., 2005). Satirapod and Wang (2000) used the same and compared SNR and satellite elevation angle.

The improvement in the stochastic models have further led to quality of ambiguity resolution and for this the many factors have been taken into account like the heteroscedastic, space- and time-correlated error structure of the GPS measurements (Wang et al., 2002). The problems of quality of GPS data from commercial softwares have been discussed in context of error modeling and quality data (Brown et al., 2002). The work has been extended to the demonstration of a geometry-free GNSS measurement analysis and the separation of different contributions to the measurement noise of pseudorange code and carrier phase observations (Bakker et al., 2009). Luo et al., (2008) developed an improved observation weighting model based on SNR measurements and showed for low elevation data additional 10% ambiguities can be resolved and the accuracy of the estimated site-specific neutrosphere parameters can be improved by nearly 25%. Recently (Yi et al., 2012) focused on this issue and outlines the research carried out to investigate the effects of some commonly used construction materials on the GPS signals.

2.2.3 Multipath mitigation

One solution for handling the multipath errors is to mitigate it. It includes not only the usage of algorithms but also design of the antenna parameters which can mitigate the multipath signals. Zhuang and Tranquilla (1995) presented the analysis of multipath and antenna effects on GPS observables using the functional modelling and simulation package of digital baseband processor for GPS receiver. To reduce code and carrier-phase multipath using GPS receiver measurements from

two or more receivers have been studied by Raquet and Lachapelle, (1996), Ray et al., (2001). To further add on it was the development of a Kalman filter for the estimation of various parameters by Ray et al., 1999, 2000b. Analyzing the generic receiver code and carrier tracking loop discriminator functions (Ray et al., 2001) formulated the relationships between receiver data and then related them to various multipath parameters. Using antenna arrays (Nayak, 2000) focused on the isolation of multipath on pseudoranges. Using the properties of time-correlation properties a technique is presented by (Yang et al., 2004). Byun et al., (2002) developed Multipath simulator taking into account reflection and diffraction (MUSTARD) to be used in the initial design phase of an experiment to identify the hazardous environmental configuration.

Code minus carrier technique has been giving effective results for effect of multipath at receiver and at times on positional accuracy by (Bisnath and Langley, 2001), (Yedukondalu et al., 2011). Satirapod and Rizos (2005) compared the semi-parametric model and new stochastic modelling techniques to mitigate the impact of systematic errors on GPS positioning, in both the theoretical and numerical sense. There have been genuine efforts to extract multipath from GPS observations. Lau and Cross (2007) made use of ray-tracing to reconstruct the multipath error to remove it. Further the experiments were made to model main multipath characteristics using GPS signals reflected from metal, water and other materials. Dual frequency carrier phase measurements method has been described by (Lee et al., 2007) using array GPS antenna system. The affects of multipath on code, SNR, and carrier phase measurements including expressions have been presented by (Axelrad et al., 2005). Further several methods for computing the correct time shift for each satellite and apply these shifts to compare code and SNR observations from day to day have been studied by (Radovanovic, 2000). To mitigate the multipath (Lee et al., 2008) used spatial statistical methods while (Rost and Wanninger, 2009) used SNR values. (Luo et al., 2008) improved observation weighting model based on signal-to noise power ratio measurements while (Bisnath and Langley, 2001) proposed an alternative method of de-weighting the affected observations based on a sentinel observable. Marais et al., (2010) developed new filtering algorithms in order to reduce inaccuracy caused by the obstacles around the receiver's antenna for intelligent traffic system while (Ge et al., 2000) found that the best multipath mitigation strategy is forward filtering using data on two adjacent days. Filtering algorithms have been used to remove multipath effects and many other improvements have been taken place (Yi et al., 2012). The references vary from prediction of satellite availability to modeling of multipath especially in urban environment. The above literature provides a strong motivation not only for the need of multipath prediction but also for the methodology to be followed.

Chapter 3: Study area, datasets, softwares and hardwares

Doon in Sanskrit and Hindi means an elongated valley. Dehradun is located in the northern part of India between latitudes 29 °58' N and 31°2'N and longitudes 77° 34' E and 78° 18'E. It is the capital of Uttarakhand state. It is located at the foothills of the Himalayas. Dehradun municipal area as per Census 2001 is 67 sq km^2 while the Census 2011 gives the population to be 578420. Dehradun is known for its natural resources, civil, defence and particularly for its prestigious educational institutions.

3.1. The study area

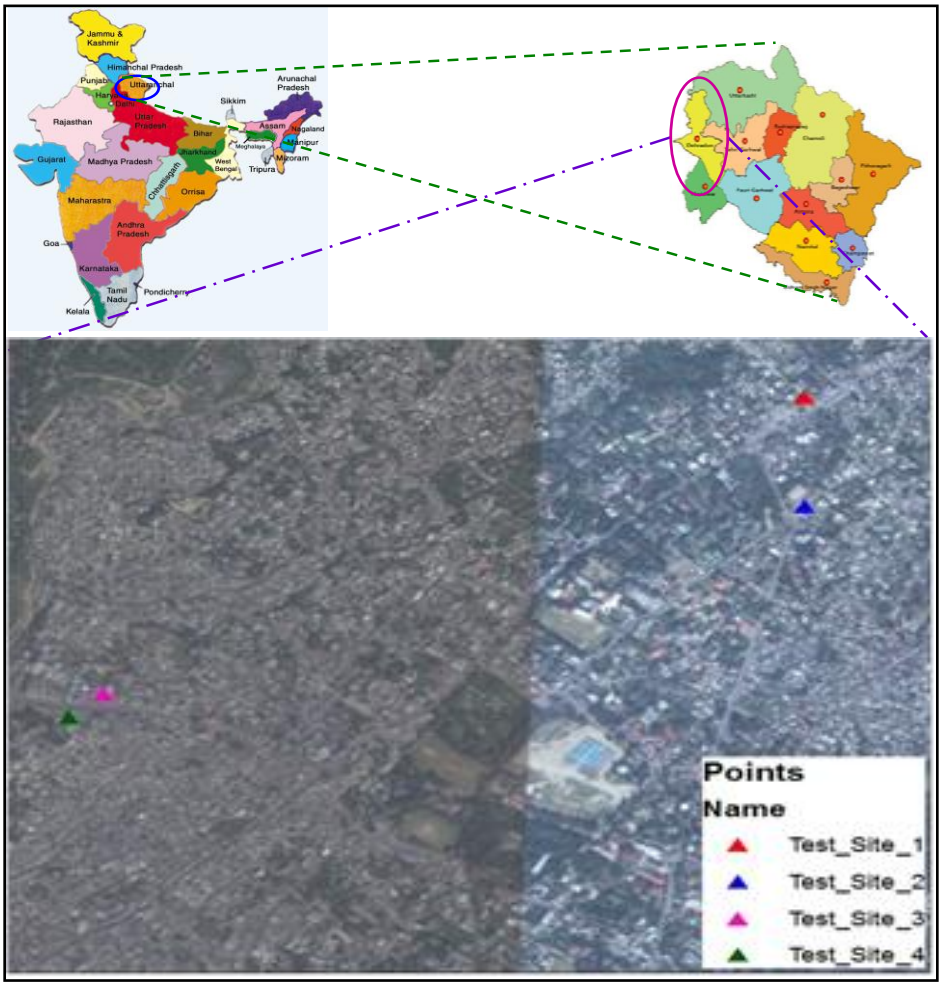

Figure 3.1 Study Area

The central part of the Dehradun is built up conventionally with dense population and is unplanned. The major development has taken place since the city became capital in 2000. Rajpur road runs from the center of the city (Clock Tower) in northern direction while Chakrata road towards west. And these are two major roads where major development has taken place. To fulfill the objectives of the

present study, an urban location is required that offers a sufficient scope of high rise buildings with different building materials and orientations. The focus is to have different urban fabric. Therefore, the areas were taken in and around in Rajpur road and Chakrata road of Dehradun city. The sites which were used for validation of the prediction model are urban geometry in IIRS campus, Raj-Plaza, Crossroads Mall, buildings behind Capri and behind LIC building. IIRS campus itself has a sufficient number of tall buildings. The buildings at the IIRS provide an urban scenario, having buildings with variable heights and different orientations. The buildings have different facades with some areas open, so it provides locations where signal may reach after getting reflected and diffracted.

(a) IIRS Campus

The next site is Raj Plaza which is on Rajpur road. The Raj plaza is a four-storey building and on right of it is another same height building separated by a road, which makes it to have an ideal location for the validation. As the two sides there are building and other two sides are open. The building has glass panes and metallic banners but majorly the buildings are of concrete only.

(b) Raj Plaza

The Crossroads mall is within 200m from Rajpur road and is on the Eastern Canal road. It is a newly built mall with shinny surfaces and has glass panes; infront of it are the houses which are of maximum two floors. The outer surface of the mall is mostly glassy. From the previous literature we know the glassy surfaces reflect more causing more of multipath signals and causing high positional error.

(c) The Crossroads Mall

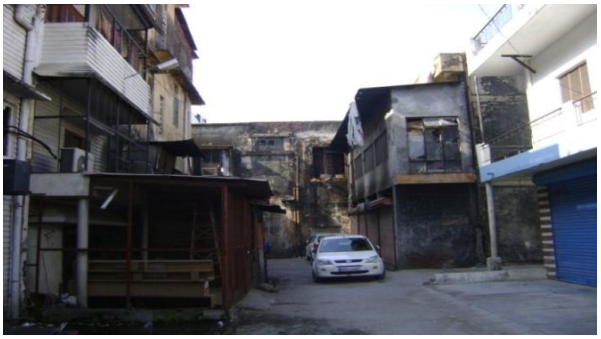

(d) Capri

(e) LIC building

Figure 3.2 Test sites

The places behind Capri and LIC building has been taken as a part of dense built-up urban environments. The study also aims to get the satellite availability in these kinds of environment. Both sides of the road exists tall buildings and the narrow lane. The buildings are old so the surface is rough, and rough surfaces attenuate the reflected signals to a higher degree. To get proper satellite geometry the DOP should be very less which is difficult to achieve in these conditions. So a proper planning is needed before going for survey in these conditions.

3.2 Datasets

The following datasets are used in this project.

3.2.1. Cartosat 1

Being the first Indian Remote Sensing Satellite capable of providing stereo images, CARTOSAT 1 is used to generate digital elevation models (DEMs), orthoimages and other products, with a spatial resolution of 2.5m. It was launched on May 05 2005. The Cartosat-1 spacecraft is configured with the panchromatic cameras which are mounted such that one camera is looking at +26 degree (fore) and the other at -5 degree (aft) along the track. These two cameras combined provide stereoscopic image pairs in the same pass. The platform is continuously steerable about spacecraft body-yaw to compensate the earth rotation correction and thus allow both fore and aft cameras to look at the same ground strip with certain time gap, this mechanisms provides stereoscopy (Krishnaswamy and Kalyanaraman).

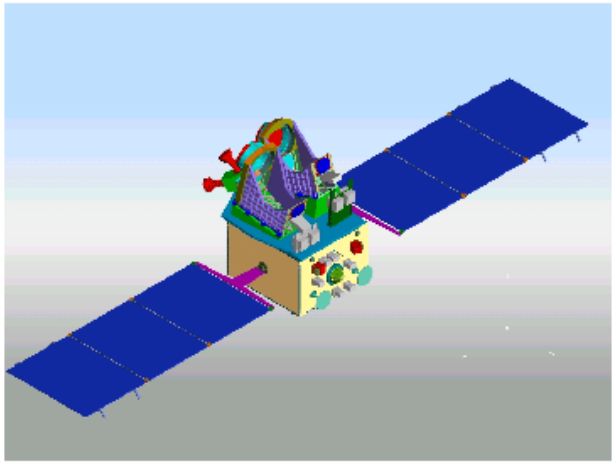

Figure 3.3 On-orbit configuration of cartosat-1 spacecraft

Table 3.1 Cartosat-1 specifications

Parameters	**Specifications**
Orbit type	Circular Polar Sun Synchronous
Orbit height	617.99 km
Orbit inclination	98.87 deg
Orbit period	97 min
Number of Orbits per day	15
Orbital Repetivity Cycle	116 days
Swath (km) (Stereo) Fore + Aft Combined (Mono)	30 km 26.855 km
Spectral Band	0.50-0.85 micron

Revisit	5 days
Attitude and Orbit Control	3-axis stabilized using Reaction Wheels, Magnetic Torquers and Hydrazine Thrusters
Radiometric resolution	10bit
Spatial Resolution: GIFOV (m) (Across-track x along-track)	2.5 x 2.78 (Fore) 2.22 x 2.23 (Aft)

3.2.1.1 Cartosat 1-DEM

The DEM used in this study has been taken from (Enkhtur, 2010).The DEM was generated using two scenes. The first scene satellite triangulation has been done with 0.7458 RMSE with 11GCPs. 15 tie points are used in the next block adjustment for both the scenes along with the 1 common GCP between these two and additional 3GCPS. Both-scene satellite triangulation has been adjusted in 1.002 RMSE with 14 GCPs. DEM was converted from pixels to ASCII file in Erdas Imagine 10.

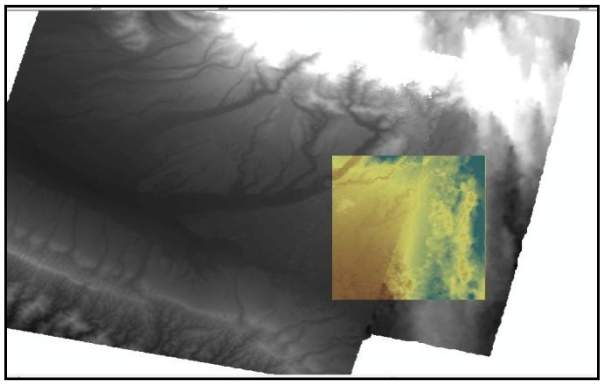

Figure 3.4 DEM generated using Cartosat-1

3.2.2. IGS Ephemeris

The IGS Ephemeris is used in this for satellite co-ordinates as discussed in section 2.1.5. In this research, the ultrarapid product was used; the program is developed to read the .sp3 file to predict the satellite availability and DOP value by calculating the elevation angle and azimuth angle which is discussed in Appendix.

3.2.3. RINEX

The data from the GPS is taken in RINEX 2.10 format discussed in section 2.1.6. In this research RINEX version 2.10 is used. The software "Convert To RINEX" utility of Trimble was used to convert from the raw data taken from Trimble R7 GNSS receiver to RINEX 2.10. The predicted SNR values were validated from the SNR extracted from the RINEX file. Also in creating the differencing models the phase values, pseudoranges and SNR values used, were taken from RINEX. For all these extraction of the various parameters from the RINEX 2.10, the program was developed in python 2.7, which can read the RINEX file and give the arranged output described in Appendix.

3.3. Softwares

The softwares and the programming language used in this project are as follows.

3.3.1. ArcGIS 10

ArcGIS 10 is a desktop GIS from ESRI. Being the major mapping component in ArcGIS, ArcMap is used to analyze, create, view and edit spatial data. ArcGlobe, ArcScene and ArcCatalog are the other components used. ArcGIS 10 was used here for the purpose of digitization and generating 3D shapefile.

3.3.2. Erdas Imagine 10

Erdas Imagine is the leading geospatial data authoring system, which incorporates remote sensing and GIS capabilities into a powerful and convenient package. It helps in generating 3D flythrough movies, cartographic-quality maps, landcover classification, orthophoto mosaics, and 2D images to name a few.

3.3.3. Python 2.7

Python has come up as powerful dynamic programming language which is being used in various domains. It is under open source license, making it freely accessible, distributable for every use. Its features are (http://www.python.org/about/).

- easy to learn, simple syntax and fast
- object oriented
- supports hierarchy
- exception based error-handling
- dynamic data types
- libraries and modules available
- easily can be integrated with other languages
- can be embedded easy within other applications
- runs on every platform

Python 2.7 was used to develop the software, its integration with ArcGIS 10 making it to use as a module.

3.4. Hardwares

The following hardwares were used in this research.

3.4.1 Trimble R7 GNSS

Trimble R7 GNSS is rugged differential GPS, modular design employing external antenna supporting L2C and L5 GPS including GLONASS. It has got varied range of surveying applications including topographic, cadastral, GCPs. Its features are (http://www.trimble.com/trimbler7gnss.shtml):

- 72-channel configurable
- External Radio configurable
- Zephyr-2 Antenna(LHCP 20dB)
- High precision L1 and L2 pseudorange measurements
- Low noise L1 and L2 carrier phase measurements
- L1 and L2 Signal-to-Noise ratios reported in dB-Hz
- Trimble low elevation tracking technology
- 24 Channels L1 C/A Code, L2C
- L1/L2 Full Cycle Carrier, WAAS/ EGNOS

Trimble R7 GNSS with Zephyr-2 geodetic antenna was used in this study. The data was stored in the receiver or survey controller.

Figure 3.5 Trimble R7 GNSS

3.4.2 Leica TPS 1201

A total station is a perfect surveying instrument combining digital theodolite and an electronic distance measuring device working together with a microprocessor to perform tasks rapidly and accurately. It can easily measure horizontal and vertical angles, slopes and distances. It also has an in-built calculator along with an electronic notebook. Leica Total Precision System (TPS) 1201 is used to get the heights and the 2-D footprint of the IIRS buildings, further leading to generation of the 3D shapefile. TPS or Total Station has many advantages is an important instrument for the surveys. One such advantage of it is attaining centimeter level accuracies. The first step is leveling and centering of the instrument. In this study back-siting method is used for setting up of the instrument in reflector mode, where the GCPs are entered.

Figure 3.6 Leica TPS 1201

The instrument is kept at the base or the reference and the reflector is taken to another point. The instrument is made to fire a laser pulse and accordingly it sets up the base. Once the base is set, the reflector mode is changed to reflector less mode and the various visible building foot prints are mapped along with heights. This process is done till all the buildings are mapped. In this research the mapping of IIRS buildings was done.

Figure 3.7 Creation of shapefile using footprints

Chapter 4: Research Methodology

4.1 Introduction

The methodology discussed here includes step by step explanation of all the procedures followed in this study. The algorithms used and the multipath prediction model developed for the urban environments are discussed in detail.

4.2 Framework of the methodology

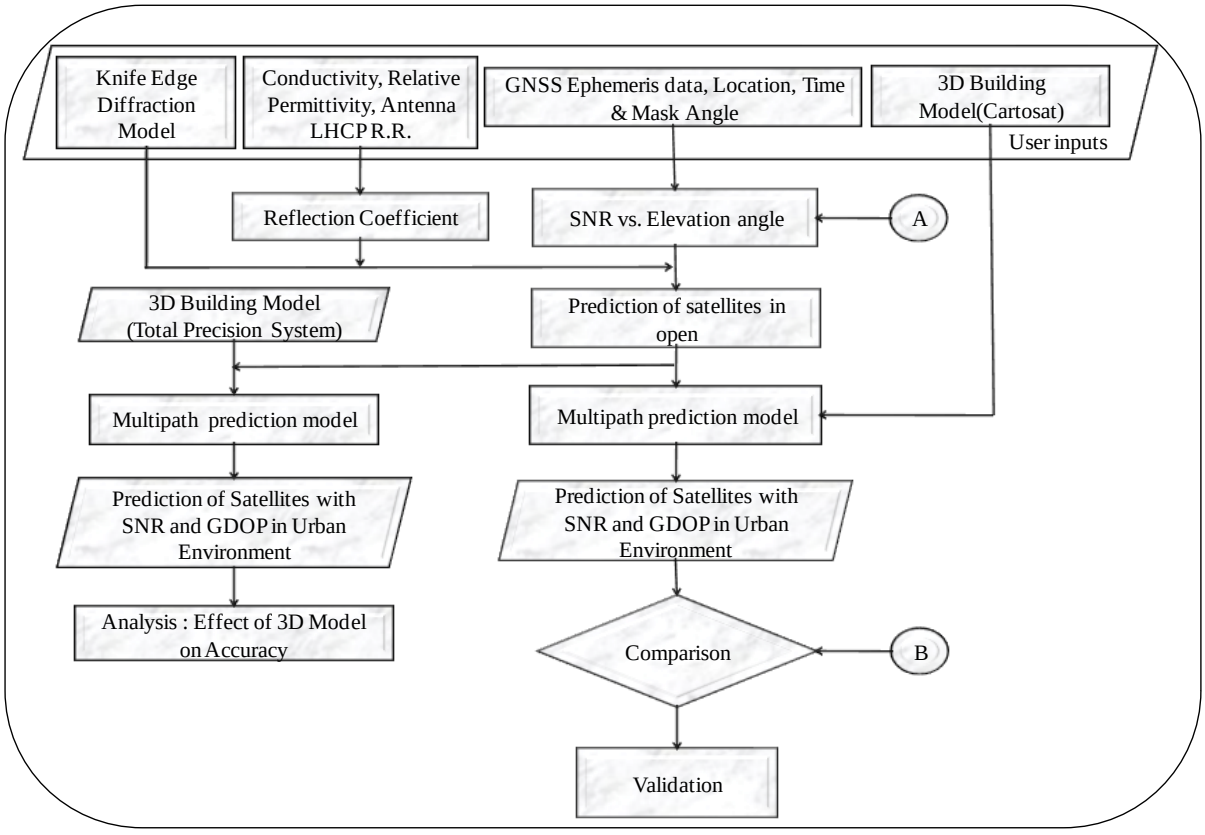

Figure 4.1 Flowchart-1 of methodology

The framework developed above is with respect to the three objectives for this work. The overall framework is depicted in Figure 4.1 and Figure 4.2. The Figure 4.1 shows basic structure of the multipath prediction model. The model incorporates for reflection and diffraction from the surfaces. Different possible multipath modes are developed for it which also accounts for LHCP R.R (rejection ratio) - a factor accounting for antenna gain pattern for multipath signals. The user needs to input the IGS ephemeris, location, mask angle and time along with 3D building model containing the electrical properties (conductivity and relative permittivity) of the building materials used. The multipath

prediction model takes 3D building model as an input, height of which has been taken from Cartosat-1 DEM (section 3.2.1.1). To analyze the effect of the accuracy of the 3D building model on the final accuracy of the model, height was also taken using TPS (section 3.4.2) and was then compared with the height from Cartosat-1.

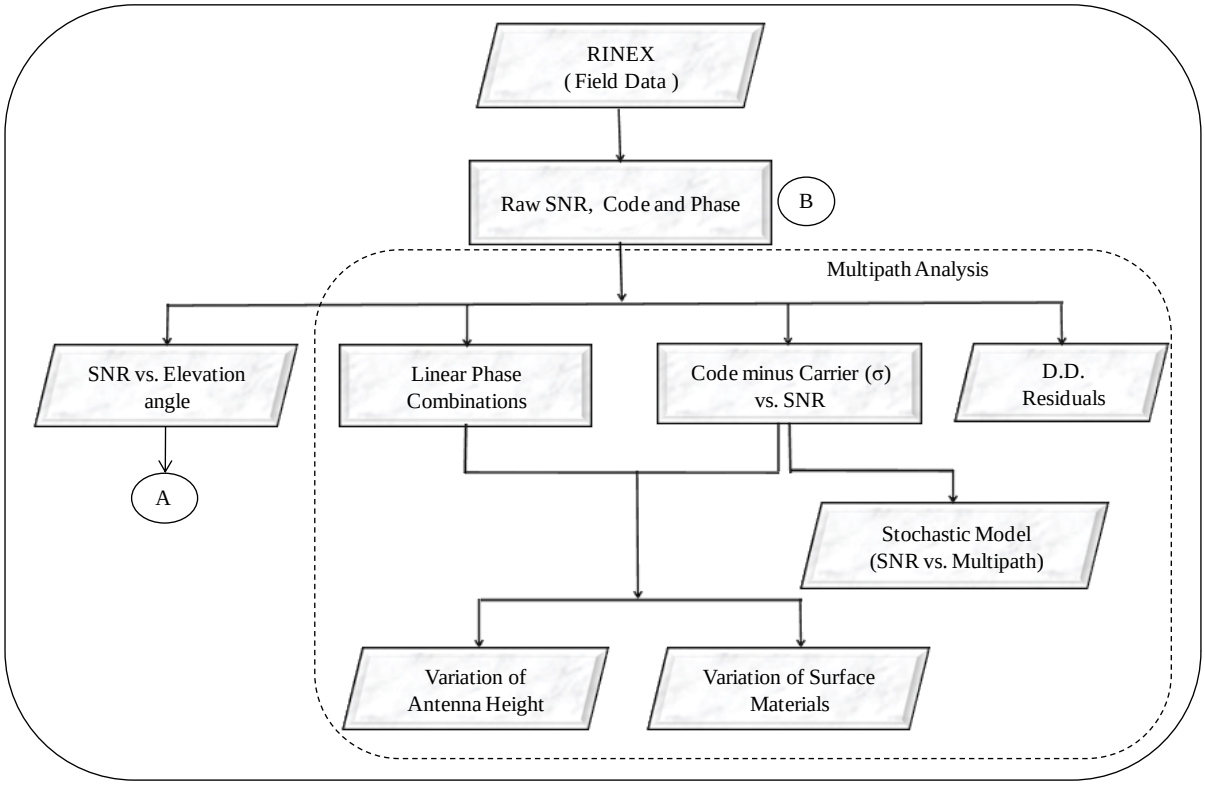

Figure 4.2 Flowchart-2 of methodology

The work has been focused to derive the relation of SNR with that of multipath errors. The raw data in RINEX format was taken at various places depicting different urban geometries. It was also taken in open conditions, over the roof top where multipath is negligible. The raw data also served the purpose of relating the SNR with that of the elevation angle. The SNR was related with that of the standard deviation of code minus phase residuals, which contains code multipath along with the noise. Thus predicting SNR can be made to comment on the GPS positional accuracy using equation 2.15. Double differencing (DD) residuals were generated using the phase observables which are free from clock errors and majorly are affected by the multipath errors and a relation of SNR with DD residuals was derived. The readings were taken at a variable GPS antenna height in order to understand the effect of antenna height on the accuracy. To analyze effect of various surface materials affecting the GPS accuracy thorough set of readings were taken for a dry and a wet surface over the roof top. The program developed for this study has proved to be handy tool at various steps during the research, be it reading a RINEX file to extract the observables or a assigning the heights to buildings taken from DEM. Especially for GPS planning, the graphical representation helps user to understand the various aspects of satellite availability and geometry.

4.3 Satellite availability and SNR prediction

A satellite is visible over an open area is decided by its elevation angle and for the urban scenario its azimuth also plays an important role in deciding the satellite visibility. GPS ephemerides were downloaded from the IGS website. GPS ephemerides are in the .sp3 format which contains the satellite coordinates in the Earth-Centered, Earth-Fixed (ECEF) format. The coordinates given by the user are in geodetic system so a conversion is needed between. The following steps were followed in software development to get the azimuth and elevation angle (Soler and Eisemann, 1994).

Step 1: The first and foremost step is to get the co-ordinates of the GPS antenna over which the satellite visibility needs to be predicted. Latitude (ϕ), longitude (λ) and height (h) of the GPS antenna are entered by the user, in geodetic co-ordinate system while the softwares takes the satellite co-ordinates from the .sp3 file entered.

Step2: Includes the conversion of co-ordinates from geodetic co-ordinate system to ECEF. The two parameters used here are semi major axis, a=6378137m defining the size of the ellipsoid and flattening f specifying shape. The terms X_u, Y_u, Z_u refer to the antenna coordinate in ECEF coordinate system.

$f^{-1} = 298.257222101 \;\; e^2 = 2f - f^2 N = \dfrac{a}{(1 - e^2 sin^2\phi)^{1/2}}$

$$X_u = (N + h)\cos(\phi)\cos(\lambda) \tag{4.1}$$

$$Y_u = (N + h)\cos(\phi)\sin(\lambda) \tag{4.2}$$

$$Z_u = (N(1 - e^2) + h)\sin(\phi) \tag{4.3}$$

Step 3: Now the conversion from ECEF to ENU (local co-ordinate system) is done to calculate the azimuth angle and elevation angle. Here the terms X_s, Y_s, Z_s refer to the satellite co-ordinates.

$X = X_s + X_u$

$Y = Y_s + Y_u$

$Z = Z_s + Z_u$

$$e = -\sin(\lambda) + \cos(\lambda)\, Y \tag{4.4}$$

$$n = -\sin(\phi)\cos(\lambda)\, X - \sin(\phi)\sin(\lambda)\, \mathrm{Y} + \cos(\phi)\, Z \tag{4.5}$$

$$u = \;\; \cos(\phi)\cos(\lambda)\, X + \cos(\phi)\sin(\lambda)\, \mathrm{Y} + \sin(\phi)\, Z \tag{4.6}$$

Step 4: Finally the Azimuth and Elevation angle are calculated using the following relations.

$$Az = \tan^{-1}\frac{e}{n} \tag{4.7}$$

$$Ele = \tan^{-1}\frac{u}{(e^2 + n^2)^{1/2}} \tag{4.8}$$

Once the elevation angle is calculated, we can predict the satellite visibility. Using the relation described in section 5.1 we can calculate the SNR of the individual satellite signal in open environment taking suitable mask angle.

4.4 Dilution of Precision (DOP)

As discussed in section 2.5.4, GDOP is also an important parameter in accuracy assessment of the GPS observations. With the predicted elevation and azimuth angle GDOP was calculated using the calculations given by (Parkinson and Spilker, 1996). The equations are as follows:

$$G = \begin{bmatrix} \cos(E_1) * \sin(Az_1) & \cos(E_1) * \cos(Az_1)\sin(E_1) & 1 \\ \cos(E_2) * \sin(Az_2) & \cos(E_2) * \cos(Az_2)\sin(E_2) & 1 \\ \cos(E_3) * \sin(Az_3) & \cos(E_3) * \cos(Az_3)\sin(E_3) & 1 \\ \cos(E_4) * \sin(Az_4) & \cos(E_4) * \cos(Az_4)\sin(E_4) & 1 \end{bmatrix} \quad (4.10)$$

$$(G^T G)^{-1} = \begin{bmatrix} (\text{East DOP})^2 & & covariance terms \\ & (\text{North DOP})^2 & \\ & & (\text{Vertical DOP})^2 \\ covariance terms & & (\text{Time DOP})^2 \end{bmatrix} \quad (4.11)$$

$$\text{HDOP} = \sqrt{(NorthDOP)^2 + (EastDOP^2)} \quad (4.12)$$

$$\text{PDOP} = \sqrt{(HDOP)^2 + (EastDOP^2)} \quad (4.13)$$

$$\text{GDOP} = \sqrt{(PDOP)^2 + (TimeDOP^2)} \quad (4.14)$$

In the above calculations, the E_i & A_i represent the elevation and the azimuth angle of the satellites visible at that epoch, the GDOP calculated is useful for the selection of best satellites.

4.5 Multipath prediction model

The model combines the reflection coefficients and diffraction coefficients discussed in section 2.1.9 and 2.1.10 to predict the satellites visible after the reflection and diffraction from the buildings. It combines the antenna gain pattern with LHCP RR and some building scenarios are generated discussed in next section.

4.5.1 Multipath modes

The three types of primary modes are taken for this research to model the GPS signal propagation in urban scenario. In the following figures, the GPS antenna height is taken as h while x is the perpendicular distance of the antenna from the building being considered (Hannah, 2001). Γ_o, Γ_x values are from equations 2.21 and 2.22.

4.5.1.1 Forward Mode

The signal reaches the GPS receiver reflecting from the ground surface. In this coupled RHCP reflection coefficient is applied directly. Path delay ΔP for this mode is $2hsin\theta$. Similarly coupled RHCP magnitude for this case is given as

$\Gamma_o + k\Gamma_x$ (4.15)

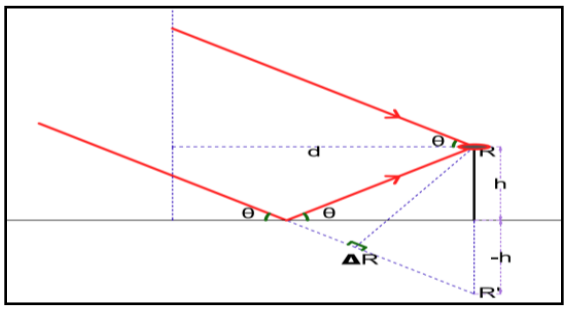

Figure 4.3 Forward mode geometry

4.5.1.2 Backward geometry

This geometry can be categorized into two, depending upon the path followed by the signal to reach the GPS receiver. When the signal is reflected striking the building and reaching directly the GPS receiver (above) it follows $h < xtan\theta$ while when the signal is reflected from ground (below) the condition followed is $h > xtan\theta$, the condition of $h = xtan\theta$ follows the corner reflection.

Above: The calculations are shown with reference to Figure 4.4. $l1\cos\theta = x\cos 2\theta$, $x = l2\cos\theta$

Path delay ΔP (l1+ l2) is $2x\cos\theta$. The magnitude of reflection coefficient for this, is calculated by taking transpose of the propagation angle in RHCP reflection coefficients which is

$\Gamma_o' + k\Gamma_x'$ (4.16)

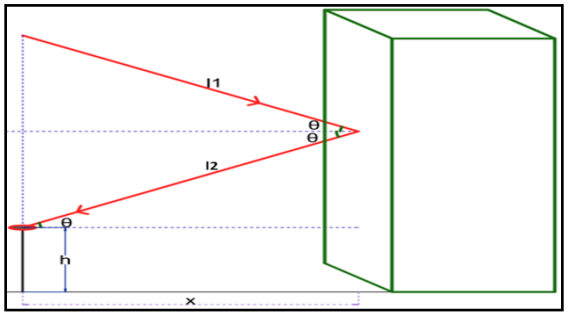

Figure 4.4 Backward geometry (Above)

Below: The backward geometry below is further discussed in two more subdivisions Model 1 (BM 1) and Model 2 (BM 2) depending upon which surface the signal strikes first ground or the building.

Model 1: The calculations are shown with reference to Figure 4.5. $x = l5 * \cos\theta$

$$l3 = 2x * \cos\theta - \frac{h * \cos 2\theta}{\sin\theta}$$

$$l4 = \frac{h}{\sin\theta} - \frac{x}{\cos\theta}$$

Path delay ΔP(l3+l4+l5) in this case is $2x\cos\theta + 2h\sin\theta$

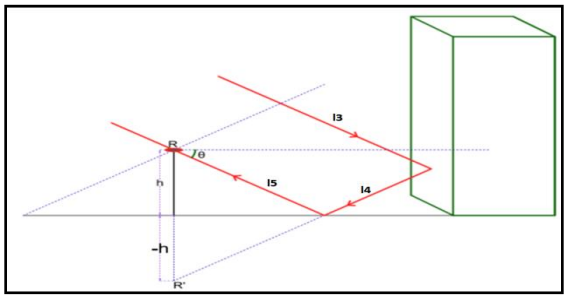

Figure 4.5 Backward geometry (BM 1)

As shown in the Figure 4.6 taking reflection coefficient for the lower surface to be ψ the effective equation becomes.

$$(\Gamma_o^{'} + k\Gamma_x^{'})\psi = \Gamma_o\Gamma_o^{'} + \Gamma_x\Gamma_x^{'} + k\Gamma_o\Gamma_x^{'} + k\Gamma_x\Gamma_o^{'}$$

Solving the above equation, we get the coupled RHCP magnitude

$$\Gamma_o + \left(\frac{k\Gamma_o^{'} + \Gamma_c^{'}}{\Gamma_o^{'} + k\Gamma_c^{'}}\right)\Gamma_x \qquad (4.17)$$

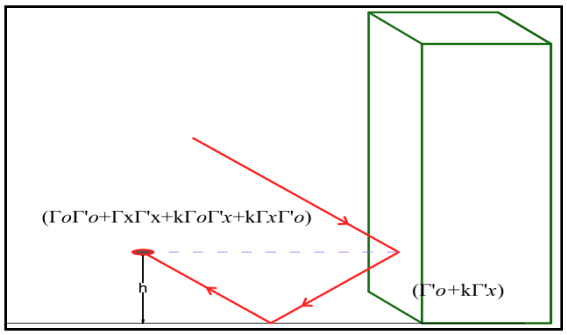

Figure 4.6 Coupled polarisation (BM 1)

The above equation equals RHCP coupled reflection magnitude of the forward geometry with its cross polarisation component is modified by ratio

$$\frac{k\Gamma_o^{'} + \Gamma_c^{'}}{\Gamma_o^{'} + k\Gamma_c^{'}}$$

Model 2: The calculations are shown with reference to Figure 4.7. $l1 * \cos\theta = x * \cos 2\theta, x = l2 * \cos\theta = l5 * \cos\theta$

$$l3 = 2x * \cos\theta - \frac{h * \cos 2\theta}{\sin\theta}$$

$$l4 = \frac{h}{\sin\theta} - \frac{x}{\cos\theta}$$

Path delay ΔP (l3+l4+l5) in this case also comes out to be

$$2x\cos\theta + 2h\sin\theta$$

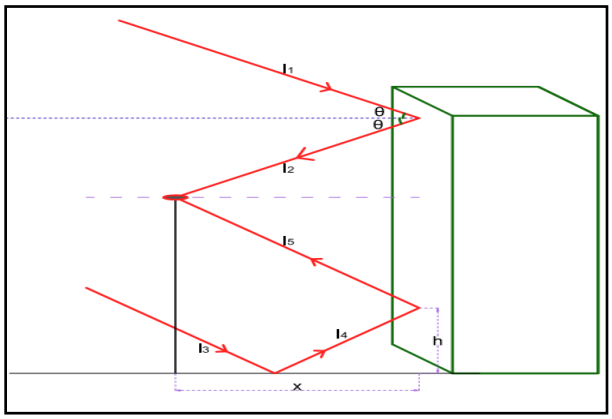

Figure 4.7 Backward geometry (BM 2)

Likewise as shown in Figure 4.8 taking the reflection coefficient to be χ, the effective equation becomes.

$$(\Gamma_o + k\Gamma_x)\chi = \Gamma_o\Gamma_o^{'} + k\Gamma_x\Gamma_o^{'} + k\Gamma_o\Gamma_x^{'} + \Gamma_x\Gamma_x^{'}$$

Solving the above equation we get the coupled RHCP magnitude

$$\Gamma_o^{'} + \left(\frac{k\Gamma_o + \Gamma_c}{\Gamma_o + k\Gamma_c}\right)\Gamma_x^{'} \qquad (4.18)$$

The above magnitude is the coupled RHCP magnitude of the backward geometry above with its cross-polarisation term modified by the ratio

$$\frac{k\Gamma_o + \Gamma_c}{\Gamma_o + k\Gamma_c}$$

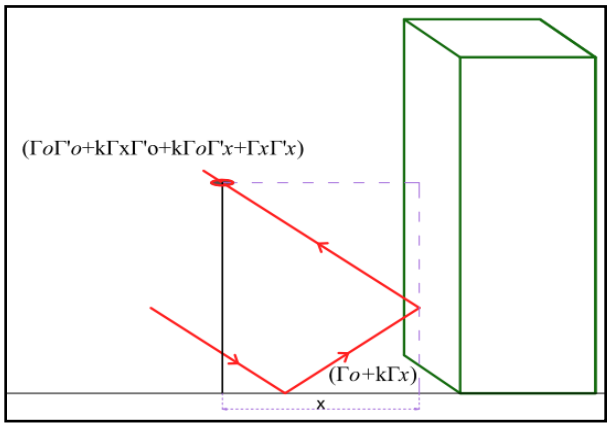

Figure 4.8 Coupled polarisation (BM 2)

4.6 Visibility Criteria

Combining all the above steps gives the output of the model. Initially all signal parameters (SNR, DOP) are predicted for an open environment. Then building model is added to it along with the reflection and diffraction coefficients and their corresponding losses in the resultant signal strength. The building model also decides if a signal will be blocked or visible.

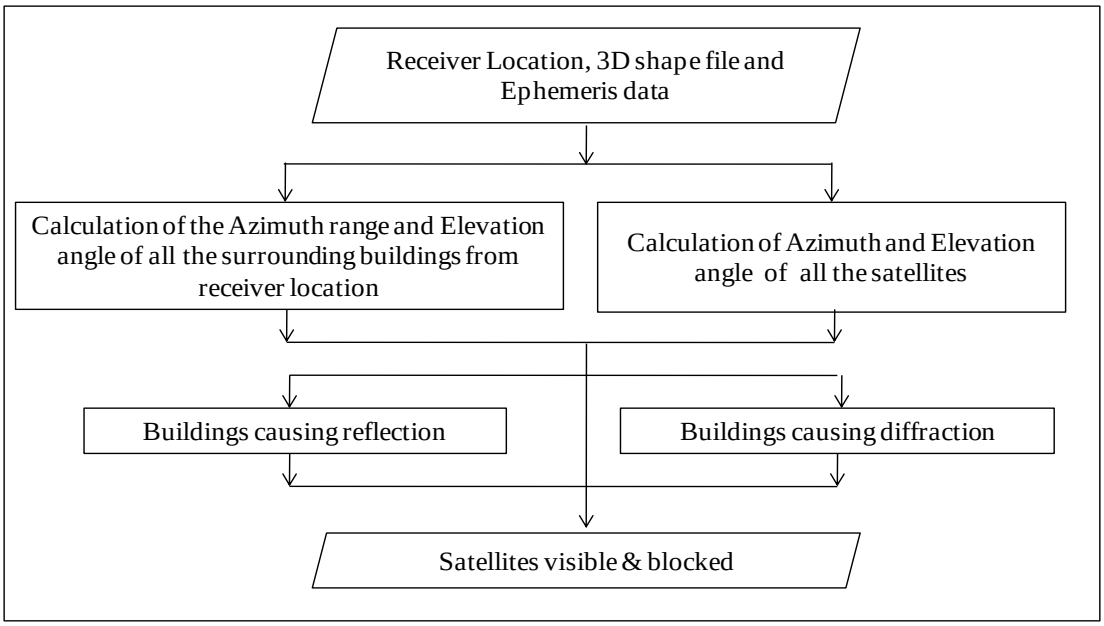

Figure 4.9 Visibility criteria

The azimuth range with respect to every building is calculated which is then compared with that of the azimuth angle of a satellite. With this information combined with that of the elevation angle with respect to building decides if that satellite will get reflected or blocked. If satellite is going to be blocked the conditions for reflection and diffraction are checked and thus it is decided if that satellite will be visible or not. The suitable propagation losses are incorporated so that the final signal strength is calculated.

4.7 Multipath Analysis

The GPS raw data is converted to a common format RINEX, which contains observed GPS observables (Pseudorange, Phase, and SNR of L1 & L2). The program developed to read RINEX 2.10 format file and provide all the observables of all the satellites extracted in a MS Excel file shown in Appendix. The SNR vs. elevation curve is plotted to get the relation between the two as discussed in section 2.1.12. The Linear phase combinations and code minus phase residuals are used to analyse the variation of antenna height and surface materials discussed in section 2.1.13 and 2.1.14. The double differencing and code minus phase residuals are used to derive the SNR relation with that of the multipath. The results are discussed in section 5.7 onwards.

4.8 Effects of building materials

Urban environment is highly random as in terms of shape, height, size, orientation, and construction material of the buildings. Multipath is affected by the reflection coefficient which is related to the material properties (conductivity and permittivity). The difference in environmental conditions may even change the reflection coefficient thus affect the accuracy. In this study a thorough readings were taken at the roof top during rainy day and a dry day at the same point. The advantage of taking roof top is there is no other multipath from surroundings than the roof surface which is sometimes dry and sometimes wet depending upon the weather. The multipath was analyzed as the variation of code minus phase vs. SNR.

The data was collected on 5/02/2013 and 8/02/2013 for 11 hrs duration each. There were heavy rains on 5/02/2013 while on 8/02/2013 it was dry. A gap of two days clearly shows the contrast in the surface conditions. The observations were taken exactly at the same point and at roof top where there is no multipath from surroundings except from that of the lower surface. So the multipath variations that are observed are due to variation in the electrical properties of the surface material, as the rain wets the concrete surface and increases its reflectivity. The orbital period of GPS constellation is of 11hours and 58 minutes which implies a satellite will be at the same location in the sky about four minutes earlier each day. This difference was incorporated in extracting the observables. Figure 4.10 and Figure 4.11 shows the wet and the dry surface.

Figure 4.10 GPS observations on Wet surface

Figure 4.11 GPS observations on Dry surface

4.9 Effect of antenna height

The antenna is one of the main component any receiver. GPS antenna receives the satellite signal and transfers it the receiver with minimum losses and maximum signal strength. Multipath can be mitigated to a certain extent using proper antenna design and better signal processing techniques. Geometry remaining the same the variation in the height of the antenna is studied to determine the suitable height at which a GPS antenna to be positioned. In this study different heights of antenna were taken at the same place so that GPS observations are taken when the urban environment is same.

(a) Antenna Height 1 m (b) Antenna Height 1.3 m (c) Antenna Height 1.6 m (d) Antenna Height 1.9 m

Figure 4.12 Test site location Capri

(a) Antenna Height 1 m (b) Antenna Height 1.4 m (c) Antenna Height 1.8 m

Figure 4.13 Test site location LIC building

In urban areas the visibility of GPS satellite is low due to the blockage, to enhance the signal reception and get more satellites visible the antenna height is increased. The observations were taken at two places behind Capri and behind LIC building discussed in Chapter 3. The antenna height behind Capri was varied for four heights 1 m, 1.3 m, 1.6 m and 1.9 m shown in Figure 4.12 with 424 observations while behind LIC building the heights varied are three 1 m, 1.4 m and 1.8 m shown in Figure 4.13 with 302 observations, with each point representing 92 epochs. A base station at a distance of 2 kms was set up over the roof so that values of rover could be compared.

Chapter 5: Results and Analysis

The chapter follows the flow of the work, covering from prediction of SNR values to development of the software which further leads to deriving the relations of the SNR with that of the Multipath residuals. Then the results predicted are validated against the results observed at different test sites. Finally the multipath modeling is discussed and the relations of the SNR and multipath are analyzed. The values are specific to Trimble R7 GNSS with Zephyr geodetic Model -2 antenna. The same relations may be similar for GLONASS and other GNSS instruments but may not be specific. Especially for the case of validation, all the results could not be shown here so values of some epochs are discussed which are found similar with the rest.

5.1 Relation of SNR and Elevation angle

A total of 6814 observations for about 11 hours were taken on 3/01/2013 and 4/01/2013. The readings were taken over the roof to get the SNR values for open environment, with both the days having bright sun with clear sky.

Figure 5.1 Test Site location at IIRS

Figure 5.2 GPS over roof taking observations

Figure 5.1 and Figure 5.2 show the location of the building and its roof where the observations were taken. As discussed in the Chapter 4 about the SNR vs. elevation angle in section 4.5.1 about a high correlation between the two, the SNR values extracted were mapped against the elevation angle. Figure 5.3 shows SNR and elevation angles. Curves Fourier with R^2 0.9596, Gaussian with R^2 0.9462, Sine function with R^2 0.9581 were fit over this data. The best fit curve found was polynomial of order 3 with co-efficient of determination R^2 to be 0.969.

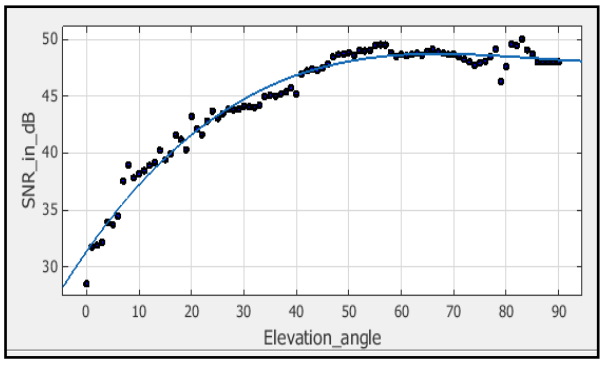

Figure 5.3 SNR vs. Elevation curve

$$SNR = 3.199 * 10^{-05} * \theta^3 - 0.0081 * \theta^2 + 0.6613 * \theta + 31.38 \quad (5.1)$$

θ represents elevation angle in the following equation. This relation has been used at various places for predicting the SNR using the predicted elevation angle. Equation 5.1 shows the relation between the SNR and the elevation angle.

5.2 3D Building model using Cartosat- DEM

DEM had an RMSE of 0.7458 as discussed in section 3.2.1.Using Pixel to ASCII conversion, an ASCII file containing the heights along with the co-ordinates was generated. The developed program takes shapefile (2D footprints of the buildings) and ASCII file as an input and gives heights of the buildings as output. Figure 5.4 shows a 3D building model developed taking the heights from the Cartosat 1 DEM.

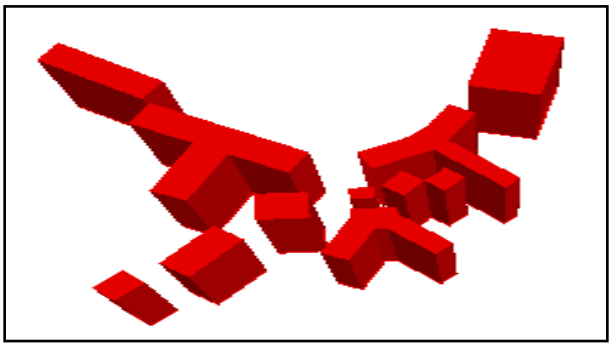

Figure 5.4 3D building model using Cartosat-DEM

5.3 Satellite availability using Viewshed analysis:

The SNR is predicted using the equation given in section 5.1, with the R^2 value to be 0.96. The developed program predicted satellite availability for base and rover. The 2D building footprints and location of base and rover is shown in Figure 5.5.The base was taken over the roof (Figure 5.6 marked in green color) and the rover was kept in front of the buildings (Figure 5.7 marked in red color).

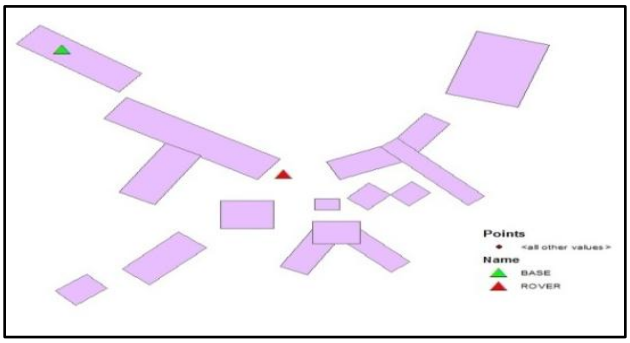

Figure 5.5 IIRS 2D-building foot prints for DGPS

On 19/09/12, a sunny day, the values were recorded for more than three hours taking 1089 observations with 10 second interval. The values were predicted using viewshed analysis, blocking a signal completely if any building comes out in its line of sight. The 3D-model was generated using Cartosat1 DEM as discussed in previous section. The visible satellites (predicted and observed) at the base and the rover are shown in Table 5.1 and Table 5.2. The base results show that the SNR values predicted are matching and the difference between observed and predicted SNR going less than 1dB. All the visible satellites could be predicted completely at the base; the difference came in SNR prediction and is more for low elevation satellites, which has less SNR, probably due to ground multipath which was not taken care at that stage. Observing the rover data, we found many satellites getting observed could not be predicted. The satellites with high SNR (>50dB) were getting predicted

and with low SNR (<35dB) ones completely getting rejected. The intermediate ones may or may not be observed.

Figure 5.6 GPS base receiver at roof top

Figure 5.7 GPS rover receiver in front of the buildings

Table 5.1 Satellites predicted and observed at BASE with SNR

Time-6.30.00	SNR				Time-7.00.00	SNR		
PRN	Observed	Predicted	Difference		PRN	Observed	Predicted	Difference
G02	44.5	43.41	1.09		G02	46.7	45.15	1.55
G04	49.5	48.34	1.16		G04	51	50.44	0.56
G08	42.8	43.89	-1.09		G08	38.6	42.07	-3.47
G09	46.8	44.39	2.41		G09	48.7	45.64	3.06
G17	50.5	48.65	1.85		G10	39.2	42.28	-3.08
G20	40.4	42.29	-1.89		G17	49.8	47.49	2.31
G26	39	42.04	-3.04		G20	39.4	42.31	-2.91
G27	47.5	45.69	1.81		G27	46.9	46.54	0.36
G28	50.2	47.71	2.49		G28	48.8	46.78	2.02

The results shown in Table 5.2 motivated to find out the cause of signal getting observed but could not getting predicted. It may be due to the positional error in the used 3D building model. It also concludes that even if a building is there obstructing the line of sight, the satellite may be visible probably due to the phenomenon of reflection and diffraction which is not taken considered at this stage.

Table 5.2 Satellites predicted and observed at ROVER with SNR

Time-6.30.00	SNR				Time-7.00.00	SNR		
PRN	Observed	Predicted	Difference		PRN	Observed	Predicted	Difference
G02	45	-----	-----		G02	48.5	------	------
G04	50.9	48.34	2.56		G04	50.7	50.44	0.26
G09	33.7	------	-----		G09	31	------	------
G17	50.9	48.65	2.25		G17	50.6	50.74	-0.14
G20	31	-------	------		G27	33.5	------	------
G28	48.7	47.71	0.99		G28	48.1	45.46	2.64

5.4 3D building model using TPS

A 3D model was generated using the heights from Total Station as discussed in section 3.4.2. In this research the mapping of IIRS buildings was done with horizontal accuracy of 40cm and vertical accuracy of 60cm. The data was transferred from instrument to the system and using Leica Geo Office software, the points were converted to the shapefile, which then was joined and corresponding height was added to every building. The model generated was used as an input to the developed multipath prediction model and thus the effect of 3D building model on the prediction of the satellite visibility and quality is compared.

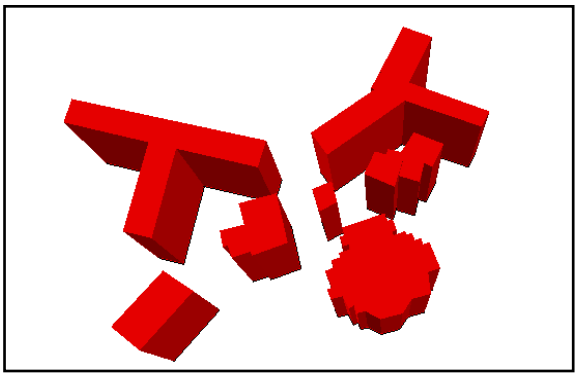

Figure 5.8 3D building model using Total Station

5.5 Satellite prediction in urban environment

Incorporating the above models of reflection and diffraction, the satellite availability and SNR have been predicted. To analyze the variation of the effect of accuracy of the 3D building model, a 3D model of IIRS was generated using Total Station. The results were then compared with the 3D building model using the Cartosat 1 DEM and the observed values are shown in Tables 5.3 (a) and (b). A total of 690 observations were taken with observation interval of 10seconds on 3/01/13, a clear sky sunny day. Observing the differences between predicted and observed SNR it could be clearly brought out that taking the height of the buildings from total station the differences are low. The major differences are at the places where the SNR is low. The maximum difference in the following table is -8.24 of both Cartosat 1 DEM and TPS, whose SNR is 34.2dB only. For PRN 24 we observe with Cartosat 1 DEM difference of 5.39 dB and for the same, with the total station the difference is 0.83dB only.

Table 5.3 Observed and predicted SNR values with 3D building model using Cartosat and Total Station

(a) Time-9.45.00

Time-9.45.00	**SNR**			**Difference(Observed-Predicted SNR)**	
	Observed	**Predicted**			
PRN		**TPS**	**Cartosat**	**TPS**	**Cartosat**
G03	40.6	41.41	41.41	-0.81	-0.81
G06	37.1	38.1	38.1	-1	-1
G14	48.8	48.74	48.74	0.06	0.06
G18	49	48.3	43.28	0.7	5.72
G19	34.2	42.44	42.44	-8.24	-8.24
G21	48	47.5	44.47	0.5	3.53
G22	50.4	48.58	48.68	1.82	1.72
G24	44.6	43.77	39.21	0.83	5.39

The PRN 18,21 22 & 24 were not visible when only plain viewshed analysis was done but after incorporating the model it was found PRN 18, 21 and 22 were visible after getting reflected from buildings while PRN 22 was visible due to diffraction. The difference in all these cases is observed to be very minimum indicating success of the model. In table 5.3 (b) too, PRN 21, 22 and 31 were not visible with plain viewshed analysis, the PRN 21, 22 were found to reach the receiver after getting reflected from the buildings while PRN31 got diffracted.

(b) Time-10.45.00

Time-10.45.00	**SNR**			**Difference(Observed-Predicted SNR)**	
	Observed	**Predicted**			
PRN		**TPS**	**Cartosat**	**TPS**	**Cartosat**
G14	50	48.77	48.77	1.23	1.23
G18	48.3	46.59	46.59	1.71	1.71
G19	45	41.05	41.05	3.95	3.95
G21	39.2	40.15	29.58	-0.95	9.62
G22	49.4	48.77	42.76	0.63	6.64
G31	48.8	45.18	43.26	3.62	5.54

Prediction accuracy of 82.60% was achieved when height was taken using Cartosat 1 DEM while using TPS prediction accuracy of 89.13% was achieved.

5.6 Test Sites:

The results at the sites chosen for this study are discussed in Table 5.4 and 5.5. A total of 316 numbers of observations were taken on 16/01/13, a sunny day. The heights were taken from the Cartosat 1 DEM. The major differences of the SNR predicted and observed were at the places where the SNR is low (<35dB). In Table 5.4, PRN 05 could be predicted but was not observed, similarly PRN 01 shown in Table 5.5. The problem was observed with satellites in the horizon (both rising and setting) which depends upon the accuracy of the ephemeris data. As shown in Figure 5.9 and Figure 5.10, PRN 05 is setting around 5.15 and PRN 01 is about to rise at 11.00. At low elevation angles, the SNR is low and ground multipath dominates which effectively reduces the signal strength and sometimes the SNR reaches to a level below the threshold for the receiver and that satellite will not be observed.

Table 5.4 Observed and predicted SNR values at RAJ Plaza

Time-5.15.00	**SNR**				**Time-5.45.00**	**SNR**		
PRN	**Observed**	**Predicted**	**Difference**		**PRN**	**Observed**	**Predicted**	**Difference**
G15	48.3	48.61	-0.31		G15	33.8	42.69	-8.89
G18	50.9	46.87	4.03		G18	49.6	43.74	5.86
G21	42.6	47.15	-4.55		G21	49.3	48.19	1.11
G26	31.6	45.61	-14.01		G22	29.4	39.29	-9.89
G29	49.9	44.92	4.98		G29	48.1	42.74	5.36
G05	-------	36.8	-------					

Table 5.5 Observed and predicted SNR values at Crossroads Mall

Time-10.45.0	SNR				Time-11.00.0	SNR		
PRN	**Observed**	**Predicted**	**Difference**		**PRN**	**Observed**	**Predicted**	**Difference**
G11	28	34.35	-6.35		G11	47.6	35.15	12.45
G14	49.3	47.49	1.81		G14	48	45.68	2.32
G18	41.8	42.63	-0.83		G18	45	40.8	4.2
G22	50.3	48.61	1.69		G22	49.2	48.37	0.83
G25	39.6	41.6	-2.00		G25	44.8	42.23	2.57
G31	49.6	48.64	0.96		G31	50.2	48.77	1.43
G01		29.65			G32	29.4	32.69	-3.29
					G01		32.22	

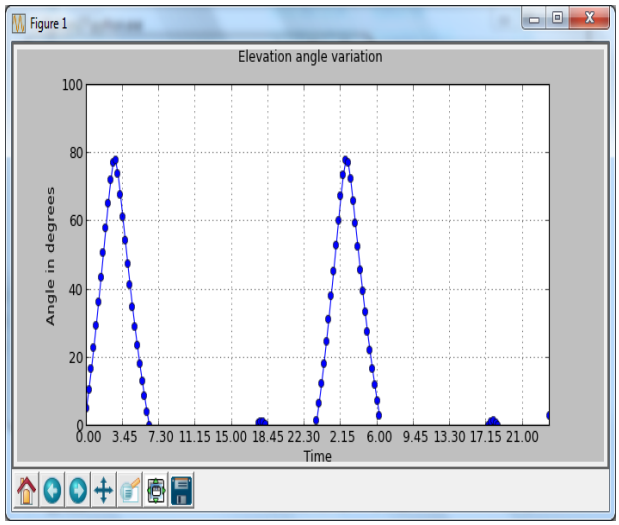

Figure 5.9 Elevation angle variation of PRN 05

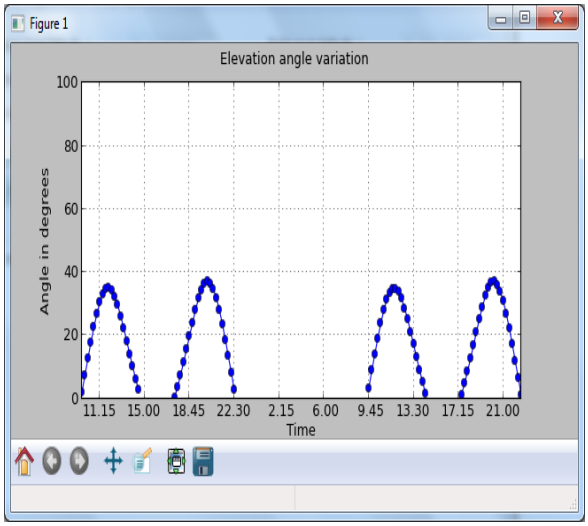

Figure 5.10 Elevation angle variation of PRN 01

5.7 Multipath Analysis

Multipath has been majorly analyzed either by using differencing models or by using some combinations of the observables. Different researchers have used different methods for quantification of the multipath. In this research, we have used code minus carrier, linear phase combinations and double differencing residuals. The observations were taken on 16/01/2013, sunny day, for more than 7 hours, with an observation interval of 10 seconds. The observations for code minus carrier and linear phase combinations were taken in standalone mode. A stochastic model generated could relate the SNR with code minus carrier residuals. A regression model was derived to analyze the DD residuals with respect to SNR values.

5.7.1 Linear Phase combinations

From the combinations discussed in section 2.1.13 the MP1 and MP2 are given by the following equations 2.26 and 2.27.

$$MP_1 = P1 - 4.0915\phi_1 + 3.0915\phi_2 + K_1 \quad (5.2)$$

$$MP_2 = \mathrm{P2} - 5.0915\phi_1 + 4.0915\phi_2 + K_2 \quad (5.3)$$

The MP1 and MP2 represent majorly the pseudorange multipath on L1 and L2. K1 and K2 being the functions of noise, integer ambiguities and multipath on carrier phase. Carrier phase multipath is negligible compared with pseudorange. Provided there is no cycle, slip K1 and K2 can be removed by averaging the data. As the P1 observable was unavailable the pseudorange multipath, C/A code on L1 (C1) was taken in place of the P1. Thus MC1 and MP2 are plotted in Figure 5.11. There were 2438 observations for PRN 22. The plot shows the multipath variations on L1 and L2 carrier frequencies on C/A code and P code.

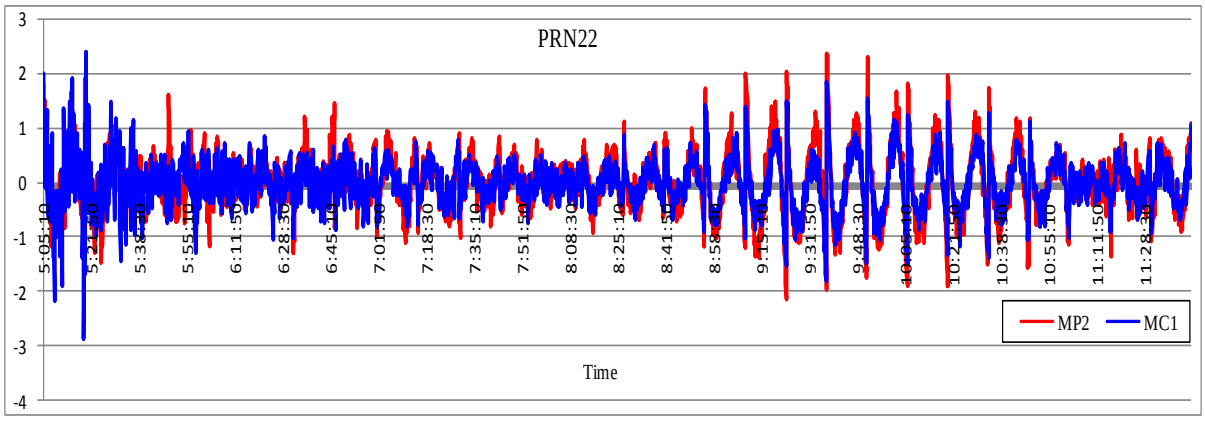

Figure 5.11 Pseudorange multipath C/A code on L1 and P code on L2 for GPS satellite PRN 22

The variations of MP2 are higher than MC1 as shown in Table 5.6. Comparing the corresponding SNR, L1 is much higher than L2 which relates SNR with multipath inversely.

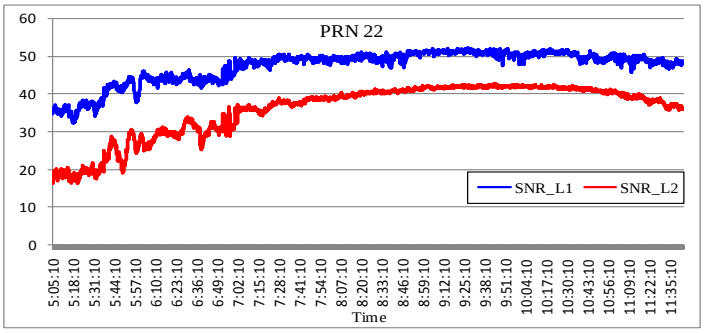

Figure 5.12 L1 and L2 SNR variation of PRN 22

Table 5.6 S.D. of Linear Phase combinations

Linear phase combination	Standard Deviation
MC1	0.4645
MP2	0.5753

5.7.2 Code minus carrier vs. SNR

The code minus carrier (C-L) linear combination is used here. The standard deviation of the C-L residuals was mapped against the average SNR. A total of 2831 observations of PRN 18 were taken with each data point representing 85 epochs. Stochastic model discussed in section 2.1.15 relates SNR with the phase noise; a similar model was derived with a mean standard deviation of observations for a 33dB-Hz R^2 between these two is 0.9520.

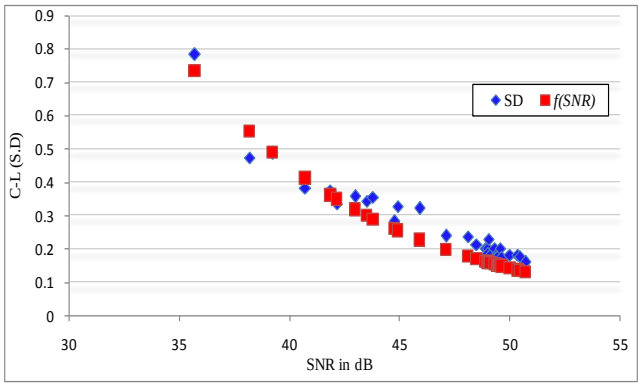

Figure 5.13 Standard deviation of C-L vs. SNR

$$\sigma_{C-L} = \frac{1}{10^{(\alpha-33)/20)}} \tag{5.4}$$

Over this data, Fourier with R^2 0.9804, Exponential with R^2 0.9712, Gaussian with R^2 0.9690 were fit to derive a relation of the standard deviation of the C-L residuals with that of the measured SNR. The best curve derived is polynomial with order 4. α represents SNR in dB in the following equations.

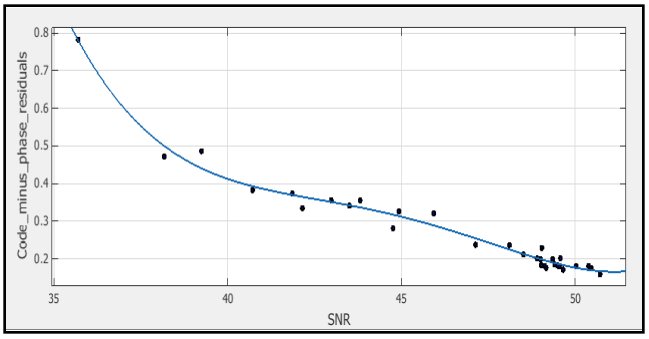

Figure 5.14 Standard deviation of C-L vs. SNR with curve fit

$$\sigma_{C-L} = 5.577 * 10^{-05}\alpha^4 - 0.01005 * \alpha^3 - 0.6785 * \alpha^2 - 20.3 * \alpha + 227.9 \tag{5.5}$$

5.8 Variation of Surface Materials

A total of 1438 observations were extracted of GPS PRN 03 for code minus carrier combination. Figure 5.15 presents the standard deviation of code minus phase of both the surfaces wet and dry with each point depicting 87 epochs (depending upon cycle shift) with the average SNR varying from 34 dB to 43 dB. It is also concluded that the difference of standard deviation of C-L residuals between the wet and the dry surface is higher at lower SNR which tends to decrease, increasing the SNR. The results show at the same place for the wet surface the multipath residuals increases more than 100% at SNR less than 34dB and 50% at SNR 37dB, than the dry one. With increase in SNR (>40dB) the effect of multipath is reduced. It also adds to the fact that in open environment surroundings the low SNR is at low elevation angles and at low elevation angles the signal reaches to the antenna from its sides where the antenna gain is minimum than on the top of the antenna where the antenna gain is maximum. On a wet day, the reflection coefficient of the ground increases which increase the

multipath signals reaching the antenna, while on the dry day the reflectivity of the surface is reduced and so is the multipath signal.

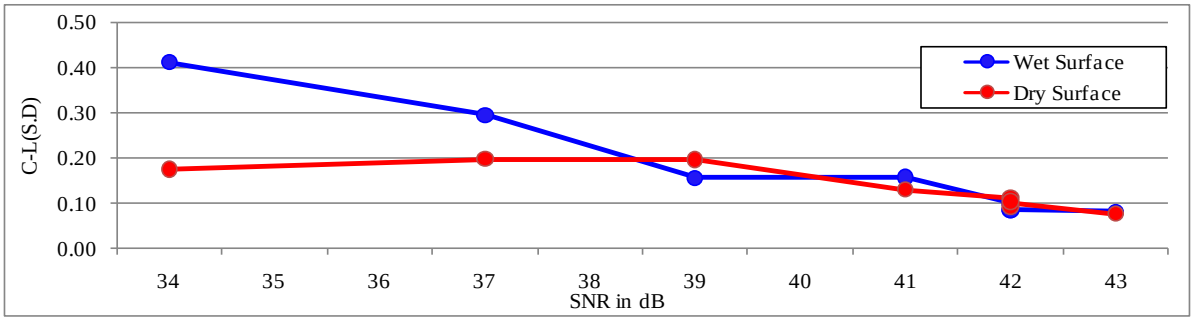

Figure 5.15 Standard deviation of C-L vs. SNR for wet and dry surface

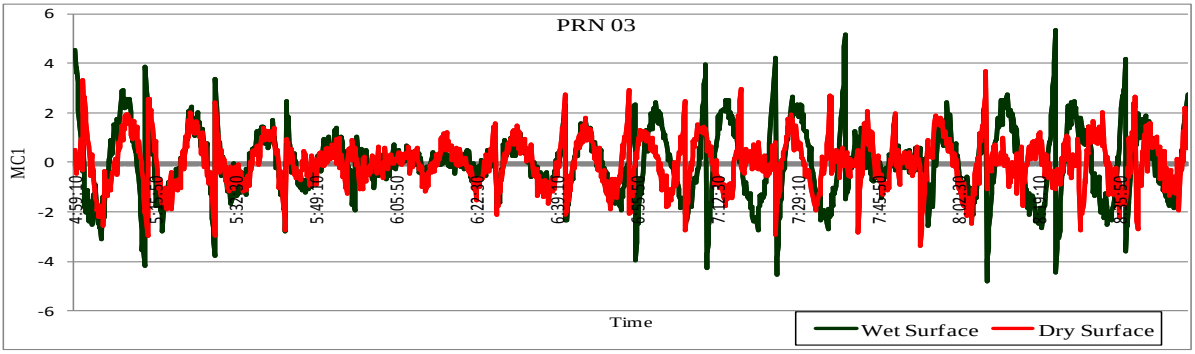

Figure 5.16 Pseudorange multipath C/A code on L1 over wet and dry surface

Over the same data 1388 observations were extracted for the linear phase multipath combination MC1, pseudorange multipath of C/A code on L1 (C1) was applied and the Figure 5.16 represents the values of MC1 with wet and the dry surfaces. The two pseudorange multipath follows a common pattern at high SNR values (>40dB) while the pattern gets shifted or scaled at low SNR during the wet day. Overall the variations are also high at wet surface, especially at the low SNR values. The corresponding SNR values are shown in Figure 5.17.

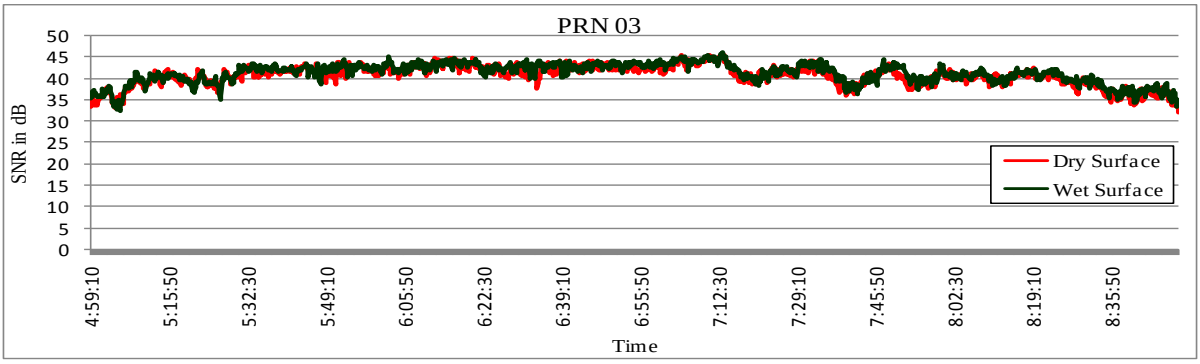

Figure 5.17 SNR variations of GPS PRN 03 on wet and the dry day

Table 5.7 S.D. pseudorange multipath due to surface materials

Type of surface	Standard Deviation
Wet	1.390734
Dry	0.981194

The values of standard deviations given in Table 5.7 further proves wet surface to have more of multipath variations. These results throw light on the effect of different construction materials used in surrounding buildings on the GPS measurement accuracy. The electrical properties (conductivity and permittivity) of different construction materials varies a lot and thus multipath variations get difficult to model in urban scenarios.

5.9 Variation of Antenna Height

The observations were taken parallely at base and rover, the standard deviation of C-L residuals was calculated of the base and rover at all the heights separately. To analyze the variation results were categorized into two. The first one, when the SNR at all the heights is nearly equal and other being at variation in SNR.

5.9.1 SNR nearly equal.

We computed the standard deviation of C-L residuals of base and the rover. Then their absolute differences were calculated. Figure 5.18 (a) shows the differences of the PRN 18 taken at four antenna heights behind Capri while Figure 5.18 (b) shows the differences of the PRN 14 taken at three antenna heights behind LIC building, both of which have low visibility being surrounded by the buildings.

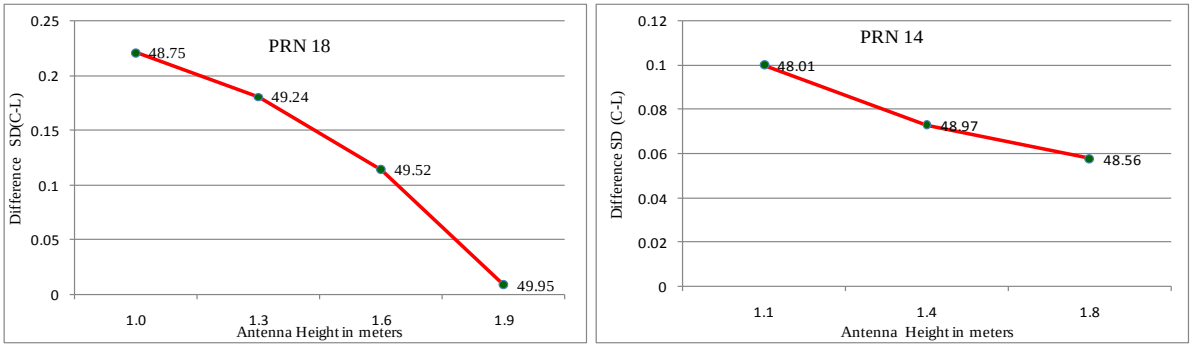

(a) PRN 18 (b) PRN 14

Figure 5.18 S.D difference of C-L residuals

The SNR in case of PRN 18 at all heights is nearly around 49 dB while that of with PRN 14 it comes out to be nearly 48dB. With increasing the antenna height, the difference between the standard deviation of C-L residuals of both the base and rover, decreases. The nearly same average SNR

implies the elevation angle also to be nearly same. So the satellites following the same elevation angle for a longer duration would follow this.

5.9.2. Variations in SNR

When the average SNR varies at each antenna height, standard deviation of C-L residuals depends mainly on SNR then on antenna height. Figure 5.19 (a) shows standard deviation C-L of the PRN 18 taken at four antenna heights. In this case, the average SNR values are nearly same and the SNR strength is also fairly good. Increasing the antenna height, decreases the multipath signals reaching the antenna, is strengthened by this graph. The standard deviation of the C-L residuals decreases with the increment in antenna height. Figure 5.19 (b) shows the same for PRN 21, in which even after increasing the antenna height the standard deviation residuals are not necessarily decreasing. The curve in this case follows the pattern influenced by the corresponding average SNR values too. Examining the first point, which has 45.72dB SNR value with 1m height has the highest standard deviation, which decreases with increasing the height and also the average value of the SNR is increased. Final point has maximum height of 1.9m but its standard deviation is more probably due to decrement in SNR. Figure 5.19 (c) shows standard deviation C-L of the PRN 22 taken at three antenna heights, behind LIC building. This graph enhances the dependence of the SNR on multipath. Infact this standard deviation curve follows the SNR variation perfectly.

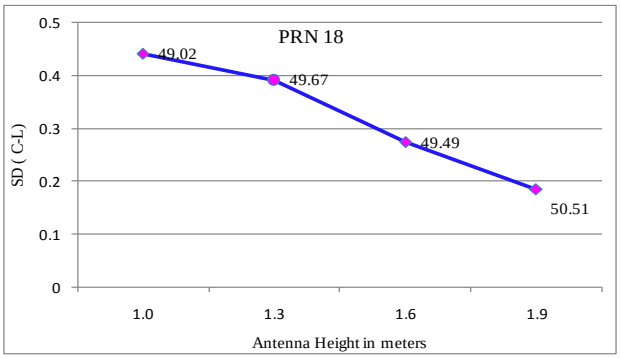

(a) PRN 18

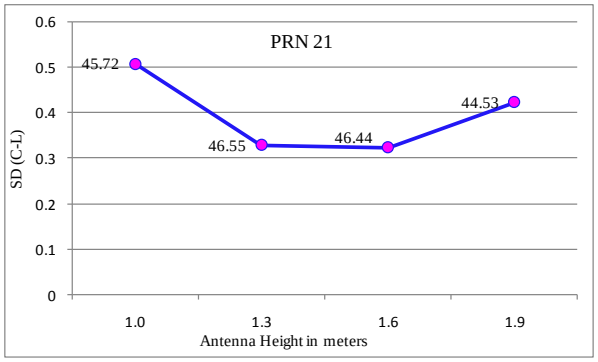

(b) PRN 21

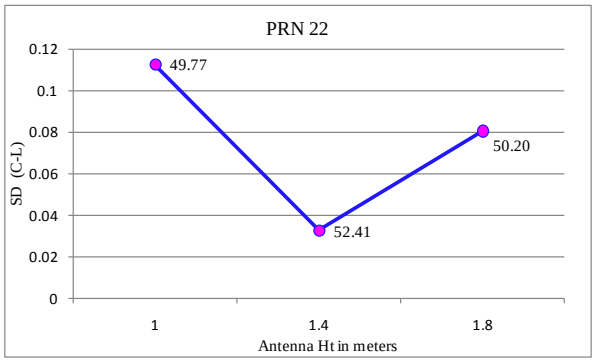

(c) PRN 22

Figure 5.19 S.D of C-L residuals

5.10 DD residuals

DD residuals require base and the rover to be observed at the same time, discussed in section 2.1.16. In this, base was setup over the building roof and the rover infront of the cross roads mall. To analyze

the DD residuals 4 GPS satellites PRN31, PRN22, PRN 25 and PRN14 were taken. Figure 5.20 depicts the DD residual with a 330 observations of PRN 31, PRN 22 pair matches with that of PRN 31, PRN 14 pair which is confirmed by the standard deviation values given in Table 5.8. The PRN 31 and PRN 22 were taken as the reference satellites as they have high SNR strength indicating them to have least multipath.

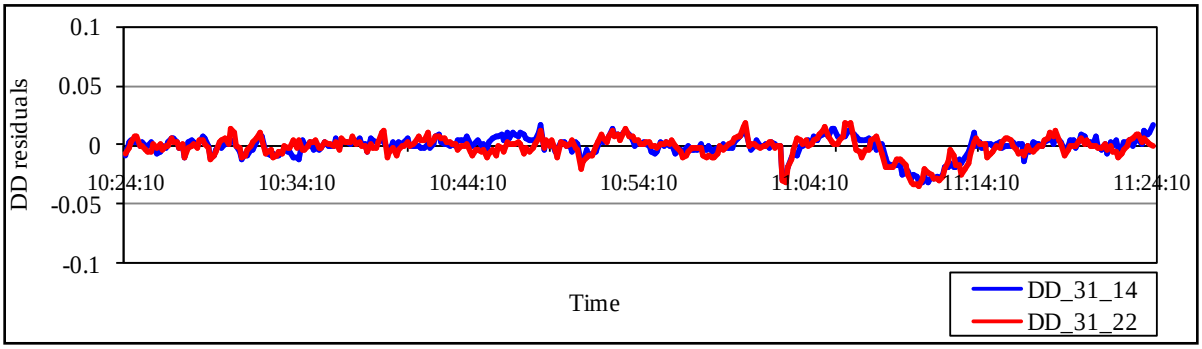

Figure 5.20 DD residuals of PRN 31, PRN 14 pair and PRN 31, PRN 22

Table 5.8 S.D. pseudorange multipath for DD pairs

Satellite pair for DD	Standard Deviation
PRN 31,22	0.0087
PRN 31,14	0.0085

From Figure 5.21 it is clear that PRN 14 has less SNR than PRN 31 and PRN 22 but always it is well above 40 dB indicating it also to be of good strength and less contaminated by multipath.

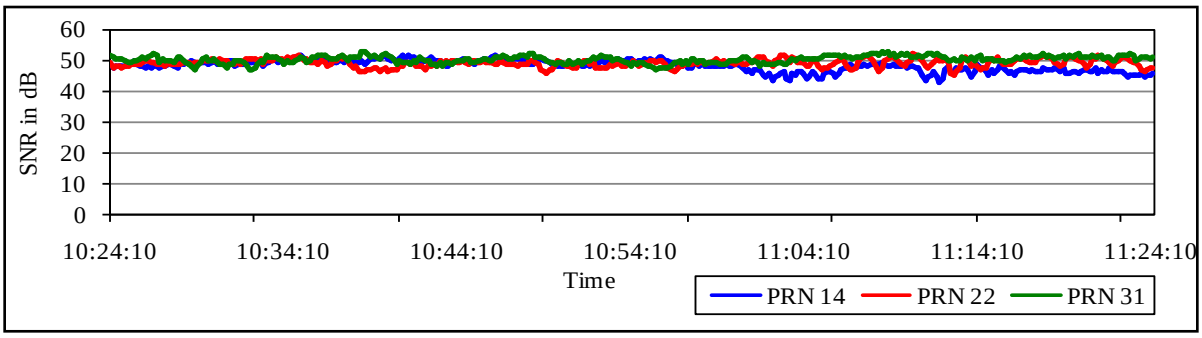

Figure 5.21 SNR in dB of PRN 31, PRN 14 and PRN 22

The other case was taken which is depicted in Figure 5.22. The DD residual with a 305 observations of PRN 31, PRN 25 pair varies much with that of PRN 31, PRN 22 pair which is confirmed by the standard deviation values shown in Table 5.9.

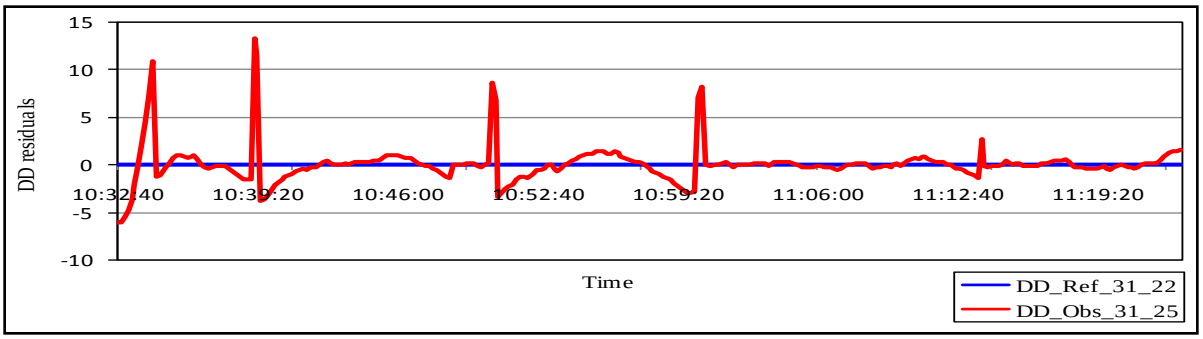

Figure 5.22 DD residuals of PRN 31, PRN 25 pair and PRN 31, PRN 22

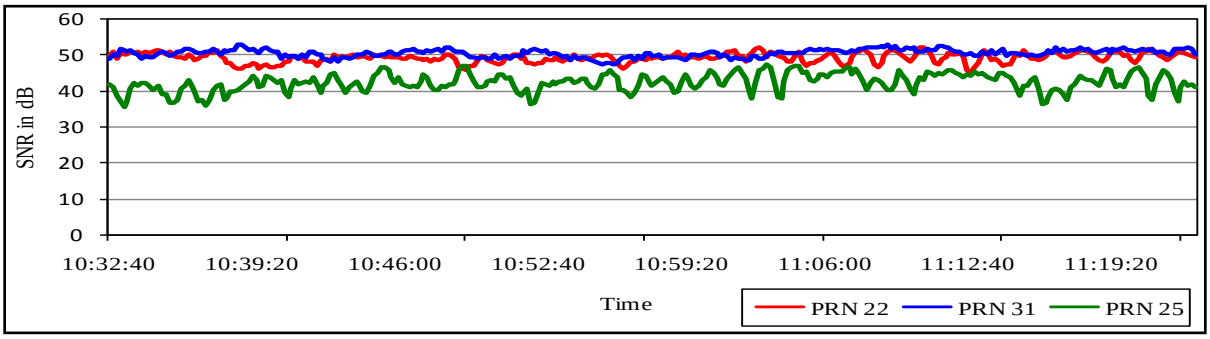

Figure 5.23 SNR in dB of PRN 31, PRN 25 and PRN 22

Table 5.9 S.D. pseudorange multipath for DD pairs

Satellite pair for DD	Standard Deviation
PRN 31,22	0.0092
PRN 31,25	1.9492

Analyzing the corresponding SNR from Figure 5.23, the SNR of PRN 25 was found to be very less compared to the rest, it dips below 40dB at many places and it never touches the SNR of the PRN 31. As DD residuals are mainly affected by multipath mainly, these results further enhance this and the role of SNR on the accuracy is clearly demonstrated. A total of 994 observations were taken for the computation of the double differencing residuals, with which the standard deviation was calculated shown in Figure 5.24. The each point depicts 55 epochs (depending upon cycle shift) and corresponding average SNR values varying from 42 to 50 dB. To derive the relation between the residuals and the SNR various curves like Polynomial with R^2 0.9433, Fourier with R^2 0.9433, Exponential with R^2 0.9245, were fit over is data.

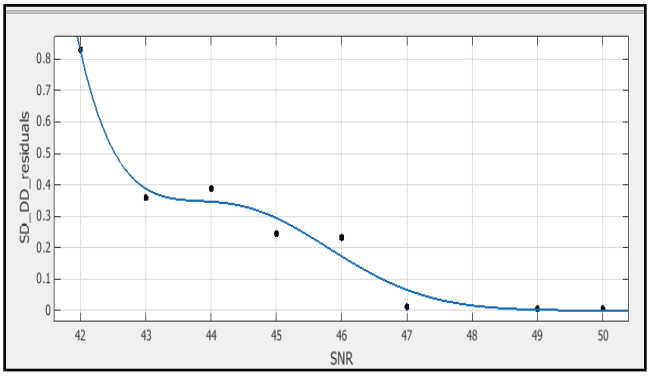

Figure 5.24 Standard deviation of DD residuals vs. SNR

$$\sigma_{DD} = 7.641 * 10^{14} * e^{\frac{-(\alpha+7.507)^2}{8.423^2}} + 0.3211 * e^{\frac{-(\alpha+44.41)^2}{1.949^2}}) \quad (5.6)$$

The best curve derived out to be Gaussian with R^2 0.9787 with the relation given in equation in (5.6). α here represents the SNR in dB. The graph shows inverse relation which is of Gaussian type between the standard deviation of the DD residuals and their corresponding SNR. The satellite availability is predicted and its SNR values which are validated successfully both for open and urban environment. In the above section, relations were derived to relate SNR with the pseudorange multipath, which further could be related to positional accuracy by the relation given in equation 2.15.

$$\sigma_{\text{Positional error}} = \text{DOP} * \sigma_{\text{pseudorange}} \quad (2.15)$$

Hence SNR proves to be an important quality indicator in GPS observables.

Chapter 6: Conclusions and Recommendations

6.1 Conclusions

This chapter summarizes the thesis work, discussing the objectives achieved and finally recommending for future work. The research related SNR with multipath and proved SNR to be an important quality indictor. Multipath prediction model was developed with a GUI and a GPS processing tool, in python. Linear phase combinations, code minus carrier and double differencing residuals were used for quantification of the multipath.

- For the prediction of satellite availability along with SNR in urban environment, the reflection and diffraction from the buildings surfaces was incorporated in the multipath prediction model.
- To analyze the signal quality in urban environment different urban geometries were incorporated with which a signal can reach to a receiver. Dry and wet surfaces were considered and results show at low SNR the multipath error increases at wet surface, which is also given by (Scappuzzo, 1997). This leads to a conclusion that surface materials affect the GPS positional accuracy significantly at low SNR.
- A strong correlation was found between SNR with elevation angle, and a polynomial regression model was derived, which was used in SNR prediction.
- A stochastic model was derived to relate the multipath residuals (code minus carrier) and SNR it was found that pseudorange multipath on L2 was higher than on CA code.
- Double differencing residuals were related with SNR having a Gaussian regression model while polynomial regression model related code minus carrier residuals with SNR.
- It was observed from the results that in urban environment increasing the antenna height may not always reduce the multipath error as it primarily depends on SNR, which is also given by (Even-Tzur and Shaked, 2008).
- A 3D building model was generated using Total Station; to analyze the effect of accuracy of 3D building model generated using Cartosat 1 DEM, on the multipath prediction model.
- A prediction accuracy of 82.6% is achieved using Cartosat 1 DEM while TPS gave an accuracy of 89.13%.
- With the analysis of the observed data it was found that to achieve high accuracy in urban environment, the SNR cut-off should not be less than 38dB, as lesser than this signal would corrupt the signal with multipath.

6.2 Recommendations

- Cartosat 1 DEM is used for 3D building shapefile as an input for the multipath prediction model but for attaining high accuracy in SNR prediction, high accuracy LiDAR data can be used.

- To analyze the antenna gain pattern of GPS antennas, a comparative study taking different GPS antennas with different LHCP rejection ratio can be carried out.
- The developed model to integrate the derived results, so that it can predict the positional accuracy along with SNR as literature provides strong relations between the two.
- A study to estimate the optimum occupation time for a given urban scenario can also be carried out using this model.
- Objects other than buildings in urban area like trees, electric poles can be incorporated in the model.

References

Alber, C., Braun, J., Rocken, C., Ware, R., 2000. Obtaining single path phase delays from GPS double differences. Am. Geophys. Union 27, 2661–266.

Axelrad, P., Larson, K., Jones, B., 2005. Use of the correct satellite repeat period to characterize and reduce site-specific multipath errors, in: Proceedings of the ION GNSS. Presented at the ION GNSS 18th International Technical Meeting of the Satellite Division, Long Beach, CA, pp. 2638–2648.

Bakker, P.F., Marel, H., Tiberius, C.C.J.M., 2009. Geometry-free undifferenced, single and double differenced analysis of single frequency GPS, EGNOS and GIOVE-A/B measurements. Gps Solutions 13, 305–314.

Beesley, B.J., 2002. Sky viewshed modeling for GPS use in the urban environment. University of South Carolina.

Ben-Moshe, B., Elkin, E., Levi, H., Weissman, A., 2011. Improving Accuracy of GNSS Devices in Urban Canyons. Presented at the 23rd Canadian Conference on Computational Geometry, 2011, Toronto ON.

Betaille, D.F., Cross, P.A., Euler, H.-J., 2006. Assessment and improvement of the capabilities of a window correlator to model GPS multipath phase errors. IEEE Trans. Aerosp. Electron. Syst. 42, 705–717.

Bilich, A., Axelrad, P., Larson, K.M., 2007. Scientific utility of the signal-to-noise ratio (SNR) reported by geodetic GPS receivers, in: Proceedings of the 20th International Technical Meeting of the Satellite Division of the Institute of Navigation ION GNSS. pp. 1999–2010.

Bilich, A., Larson, K.M., 2007. Mapping the GPS multipath environment using the signal-to-noise ratio (SNR). Radio Sci. 42, n/a–n/a.

Bilich, A., Larson, K.M., Axelrad, P., 2004. Observations of signal-to-noise ratios (SNR) at geodetic GPS site CASA: Implications for phase multipath. Proc. Cent. Eur. Geodyn. Seism. 23, 77–83.

Bisnath, S.B., Langley, R.B., 2001. Pseudorange multipath mitigation by means of multipath monitoring and de-weighting, in: Proceedings of the International Symposium on Kinematic Systems in Geodesy, Geomatics and Navigation. Banff, Alberta, pp. 392–400.

Bouchiat, M.A., Guéna, J., Jacquier, P., Lintz, M., Papoyan, A.V., 1999. Electrical conductivity of glass and sapphire cells exposed to dry cesium vapor. Appl. Phys. B 68, 1109–1116.

Bradbury, J., 2008. The Integration of City Models and GNSS for the Simulation and Modelling of Multipath and Availability: Paving the Way for New Applications. University College London, London.

Brown, N., Kealy, A., Williamson, I., 2002. Stochastic Modelling of GPS Phase Observations for Improved Quality Estimation. Cartography 31, 143–151.

Byun, S.H., Hajj, G.A., Young, L.E., 2002. Development and application of GPS signal multipath simulator. Radio Sci. 37, 10–1–10–23.

Cederholm, P., 2010. Statistical characteristics of L1 carrier phase observations from four low-cost GPS receivers. Nord. J. Surv. Real Estate Res. 7.

Collins, J.P., Langley, B.L., 1999. Possible Weighting Schemes for GPS Carrier Phase Observations in the Presence of Multipath.

Dana, P.H., 1997. Global Positioning System Overview. Ncgia Core Curric. Giscience.

Dierendonck, van, Parkinson, B.., Spilker Jr, J.J., 1996. GPS Receivers, in: Global Positioning System: Theory and Applications. American Institute of Aeronautics and Astronautics, Washington DC, pp. 329–408.

Ebner, A., 2008. On the attainable accuracy of multi-system GNSS positioning in high-multipath urban environments.

Enkhtur, B., 2010. Topographic Database Extraction at 1:25000 Using CARTOSAT-1 Stereo Data, CSSTEAP14th RS&GIS Post Graduate Diploma course. Indian Institute of Remote Sensing (NRSC), Dehradun.

Esteban Vázquez B, G., Grejner-Brzeziska, D.A., 2012. A case of study for Pseudorange multipath estimation and analysis: TAMDEF GPS network. Geofísica Int. 51, 63–72.

Estey, L.H., Meertens, C.M., 1999. TEQC: The Multi-Purpose Toolkit for GPS/GLONASS Data. Gps Solutions 3, 42–49.

Even-Tzur, G., Shaked, D., 2008. GPS Antenna Height and Its Influence on Pseudorange Multipath, in: TS 5G - GNSS Antenna Calibration and Accuracy Assessment. Presented at the Integrating Generations FIG Working Week 2008 Stockholm, Sweden, p. 12.

Fan, K., Ding, X., 2006. Estimation of GPS carrier phase multipath signals based on site environment. J. Glob. Position. Syst. 5, 22–28.

Fante, R.L., Vaccaro, J.J., 2003. Evaluation and reduction of multipath-induced bias on GPS time-of-arrival. Ieee Trans. Aerosp. Electron. Syst. 39, 911–920.

Fantino, M., Dovis, F., Wang, J., Fantino, P.M., 2004. Quality Monitoring for Multipath Affected GPS Signals.

Fresnel, A.J., 2001. Plane W aves and W ave Propagation. Louisiana State University Book.

García, J.G., Mercader, P.I., Muravchik, C.H., 2005. Use of GPS carrier phase double differences. Lat. Am. Appl. Res. 35, 115–120.

Ge, L., Han, S., Rizos, C., 2000. Multipath Mitigation of Continuous GPS Measurements Using an Adaptive Filter. Gps Solutions 4, 19–30.

Ge, L., Han, S., Rizos, C., 2002. GPS multipath change detection in permanent GPS stations. Surv. Rev. 36, 306–322.

Gurtner, W., 2007. RINEX: The Receiver Independent Exchange Format Version 2.10. Astronomical Institute, University of Berne.

Hannah, B.M., 2001. Modelling and simulation of GPS multipath propagation. Queensland University of Technology, Queensland.

Huber, K., Heuberger, F., Abart, C., Karabatic, A., Weber, R., Berglez, P., 2010. PPP: Precise Point Positioning – Constraints and Opportunities, in: TS 10C - GNSS Modernisation and Trends. Presented at the TS 10C - GNSS Modernisation and Trends, Sydney.

Iyiade, A., 2005. Real Time Kinematic GPS in an Urban Canyon Environment. Presented at the Map Asia 2005, Jakarta, Indonesia.

Kim, D., Langley, R.B., n.d. The Multipath Divergence Problem in GPS Carrier-Smoothed Code Pseudorange.

Kirchner, M., Becker, M., 2005. The Use of Signal Strength Measurements for Quality Assessments of GPS Observations. Reports Geod. 73.

Kraus, J.D., Carver, K.R., 1973. Electromagnetics, Second. ed. McGraw-Hill Book Company.

Krishnaswamy, M., Kalyanaraman, S., n.d. Indian Remote Sensing Satellite Cartosat-1: Technical features and data products.

Langley, R.., Teunissen, P.J.G., Kleusberg, A., 1998. GPS Receivers and the Observables, GPS for Geodesy. Springer, Berlin.

Lau, L., Cross, P., 2007. Development and testing of a new ray-tracing approach to GNSS carrier-phase multipath modelling. J. Geod. 81, 713–732.

Lee, E., Chun, S., Lee, Y.J., Kang, T., Jee, G., Kim, J., 2007. Parameter estimation for multipath error in GPS dual frequency carrier phase measurements using unscented Kalman filters. Int. J. Control Autom. Syst. 5, 388–396.

Lee, Y.-W., Suh, Y.-C., Shibasaki, R., 2008. A simulation system for GNSS multipath mitigation using spatial statistical methods. Comput. Geosci. 34, 1597–1609.

Li, J., Taylor, G., Kidner, D., Ware, M., 2008. Prediction and visualization of GPS multipath signals in urban areas using LiDAR Digital Surface Models and building footprints. Int J Geogr Inf Sci 22, 1197–1218.

Luo, X., Mayer, M., Heck, B., 2008. Improving the Stochastic Model of GNSS Observations by Means of SNR-based Weighting, in: Sideris, M.G. (Ed.), Observing Our Changing Earth, International Association of Geodesy Symposia. Springer Berlin Heidelberg, pp. 725–734.

Marais, J., Berbineau, M., Heddebaut, M., 2005. Land mobile GNSS availability and multipath evaluation tool. Ieee Trans. Veh. Technol. 54, 1697–1704.

Marais, J., Duflos, E., Viandier, N., Nahimana, D.F., Rabaoui, A., 2010. Advanced signal processing techniques for multipath mitigation in land transportation environment, in: 2010 13th International IEEE Conference on Intelligent Transportation Systems (ITSC). Presented at the 2010 13th International IEEE Conference on Intelligent Transportation Systems (ITSC), pp. 1480–1485.

Mekik, C., Can, O., 2010. Multipath Effects in RTK GPS and a Case Study, in: A. Presented at the 2010 International Symposium on GPS/GNSS, Taipei, Taiwan, pp. 231–239.

Nayak, R.A., 2000. Reliable and Continuous Urban Navigation Using Multiple GPS Antennas and a Low Cost IMU. Calgary, Alberta.

O'Shaughnessy, E., 2012. The UNSW@ ADFA Journal of Undergraduate Engineering Research, Vol 5, No 1 (2012).

Obst, M., Bauer, S., Reisdorf, P., Wanielik, G., 2012. Multipath detection with 3D digital maps for robust multi-constellation GNSS/INS vehicle localization in urban areas, in: 2012 IEEE Intelligent Vehicles Symposium (IV). Presented at the 2012 IEEE Intelligent Vehicles Symposium (IV), pp. 184–190.

Park, K.-D., Davis, J.L., Jarlemark, P.O., Elosegui, P., Normandeau, J.E., Corey, B.E., Niell, A.E., Meertens, C.E., Andreatta, V.A., 2002. Multipath characteristics of GPS signals as determined from the Antenna and Multipath Calibration System, in: ION GPS 2002: 15 Th International Technical Meeting of the Satellite Division of The Institute of Navigation.

Parkinson, B.W., Spilker, J.J., 1996. Global Positioning System: Theory and Applications (volume One). AIAA.

Radovanovic, R., 2000. High accuracy deformation monitoring via multipath mitigation by day-to-day correlation analysis, in: Proceedings of the 13th International Technical Meeting of the Satellite Division of the Institute of Navigation. pp. 35–44.

Raquet, J., Lachapelle, G., 1996. Determination and reduction of GPS reference station multipath using multiple receivers, in: PROCEEDINGS OF ION GPS. pp. 673–681.

Ray, J.K., 2000a. Mitigation of GPS code and carrier phase multipath effects using a multi-antenna system. University of Calgary.

Ray, J.K., 2000b. Mitigation of GPS code and carrier phase multipath effects using a multi-antenna system. University of Calgary.

Ray, J.K., Cannon, M.E., Fenton, P., 2001. GPS code and carrier multipath mitigation using a multiantenna system. Aerosp. Electron. Syst. IEEE Trans. 37, 183–195.

Ray, J.K., Cannon, M.E., Fenton, P.C., 1999. Mitigation of static carrier-phase multipath effects using multiple closely spaced antennas. Navig.-Wash. 46, 193–202.

Richter, B., Euler, H.J., 2001. Study of Improved Observation Modeling for Surveying Type Applications in Multipath Environment. Presented at the Proceedings of the 14th International Technical Meeting of the Satellite Division of The Institute of Navigation (ION GPS 2001), pp. 1048–1055.

Rost, C., Wanninger, L., 2009. Carrier phase multipath mitigation based on GNSS signal quality measurements. J. Appl. Geod. 3.

Satirapod, C., Rizos, C., 2005. Multipath mitigation by wavelet analysis for GPS base station applications. Surv. Rev. 38, 2–10.

Satirapod, C., Wang, J., 2000. Comparing the quality indicators of GPS carrier phase observations. Geomatics Res. Australas. 73, 75–92.

Scappuzzo, F.S., 1997. Phase multipath estimation for global positioning system (GPS) using signal-to-noise-ratio (SNR) data (Thesis). Massachusetts Institute of Technology.

Schubert, F., Prieto-Cerdeira, R., Steingass, A., 2008. GNSS Software Simulation System for Realistic High-Multipath Environments, in: Proceedings of the 4th ESA Workshop on Satellite Navigation User Equipment Technologies (Navitec 2008). Presented at the 4th ESA Workshop on Satellite Navigation User Equipment Technologies (Navitec 2008), Noordwijk, Niederlande.

Serrano, L., Kim, D., Langley, R.B., 2005. A new carrier-phase multipath observable for GPS real-time kinematics, based on between receiver dynamics. Proc Annu Meet Inst Navig 1105–1115.

Soler, T., Eisemann, D.W., 1994. Determination of look angles to geostationary communication satellites. J. Surv. Eng. 120, 115–127.

Soubielle, J., Fijalkow, I., Duvaut, P., Bibaut, A., 2002. GPS positioning in a multipath environment. Ieee Trans. Signal Process. 50, 141–150.

SUH, Y., LEE, Y.-W., SHIBASAKI, R., n.d. Web 2.0 gis for the simulation of GNSS availability in urban areas.

Taylor, G., Li, J., Kidner, D., Brunsdon, C., Ware, M., 2007. Modelling and prediction of GPS availability with digital photogrammetry and LiDAR. Int. J. Geogr. Inf. Sci. 21, 1–20.

Taylor, G., Li, J., Kidner, D., Ware, M., 2005. Surface Modelling for GPS Satellite Visibility, in: Li, K.-J., Vangenot, C. (Eds.), Web and Wireless Geographical Information Systems, Lecture Notes in Computer Science. Springer Berlin Heidelberg, pp. 281–295.

Verhagen, S., 2005. The GNSS integer ambiguities: estimation and validation. NCG, Nederlandse Commissie voor Geodesie, Netherlands Geodetic Commission, Delft, Netherlands.

Wang, J., Satirapod, C., Rizos, C., 2002. Stochastic assessment of GPS carrier phase measurements for precise static relative positioning. J. Geod. 76, 95–104.

Wieser, A., Gaggl, M., Hartinger, H., 2005. Improved positioning accuracy with high sensitivity GNSS receivers and SNR aided integrity monitoring of pseudo-range observations, in: Proc ION GNSS. Presented at the ION GNSS 18th International Technical Meeting of the Satellite Division, Long Beach, CA, pp. 13–16.

Wilson, R., 2002. Propagation Losses Through Common BuildingMaterials 2.4 GHz vs 5 GHz. University of Southern California, California.

Yang, Y., Hatch, R.R., Sharpe, R.T., 2004. GPS Multipath Mitigation in Measurement Domain and Its Applications for High Accuracy Navigation, in: Proceedings of the 17th International Technical Meeting of the Satellite Division of The Institute of Navigation (ION GNSS 2004). Long Beach, CA, pp. 1124 – 1130.

Yedukondalu, K., Sarma, A.D., Srinivas, V.S., 2011. Estimation and mitigation of GPS multipath interference using adaptive filtering. Prog. Electromagn. Res. M 21, 133–148.

Yi, T.-H., Li, H.-N., Gu, M., 2012. Effect of different construction materials on propagation of GPS monitoring signals. Measurement 45, 1126–1139.

Zajícek, R., Vrba, J., 2010. Broadband Complex Permittivity Determination for Biomedical Applications. Adv. Microw. Circuits Syst.

Zheng, S.Y., 2005. Signal acquisition and tracking for a software GPS receiver. Virginia Polytechnic Institute And State University.

Zhuang, W., Tranquilla, J.M., 1995. Effects of multipath and antenna on GPS observables. Radar Sonar Navig. Iee Proc. - 142, 267–275.

Zinas, D.N., 2011. GPS Network RTK Tutorial (No. TEKMON-001). Tekmon Geomatics LLP.

Appendix

Program developed

The codes generated for various tasks were integrated into software named "GNSS data processing". Figure 1.1 shows GUI of the software developed. The submenus developed are Rinexe, Ephemeris and 3D_Shapefile. The validation of the results predicted is discussed in section 5.6.The software developed uses ephemeris file and other similar programs use the almanac data as an input.

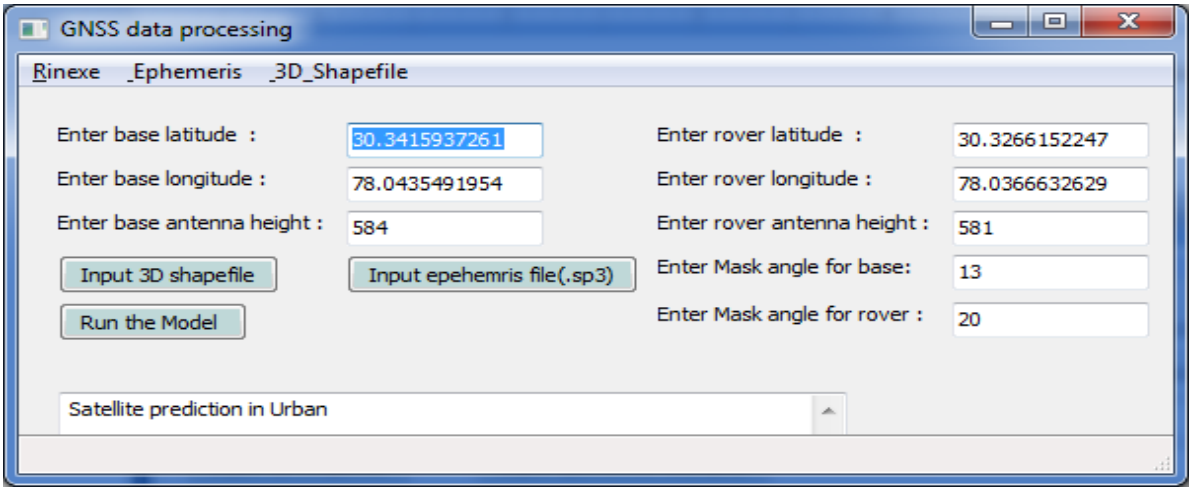

Figure 1.1 GUI of the software "GNSS data processing" developed

Satellite prediction in urban environment

The satellite prediction model takes inputs as base, rover location, 3D shapefile, ephemeris data and the mask angle. A text box is developed for base, rover location and also to add mask angle. With the buttons 3D shapefile and ephemeris file can be entered. Running the model takes all the above conditions discussed of reflection and diffraction, calculates the loss due to it in SNR and predicts the SNR for urban environment. The outputs are generated in notepad file and are stored in three different folders. The first folder contained the visible satellites with their PRN No, SNR and elevation angle of base and rover both. For every epoch one such notepad file shown in Figure 1.2 is created. The base is predicted with satellites at open while for the rover the satellites are predicted considering the surroundings, incorporating the reflecting and diffraction from the surrounding buildings. This output can be very helpful for DGPS –planning especially in urban environment.

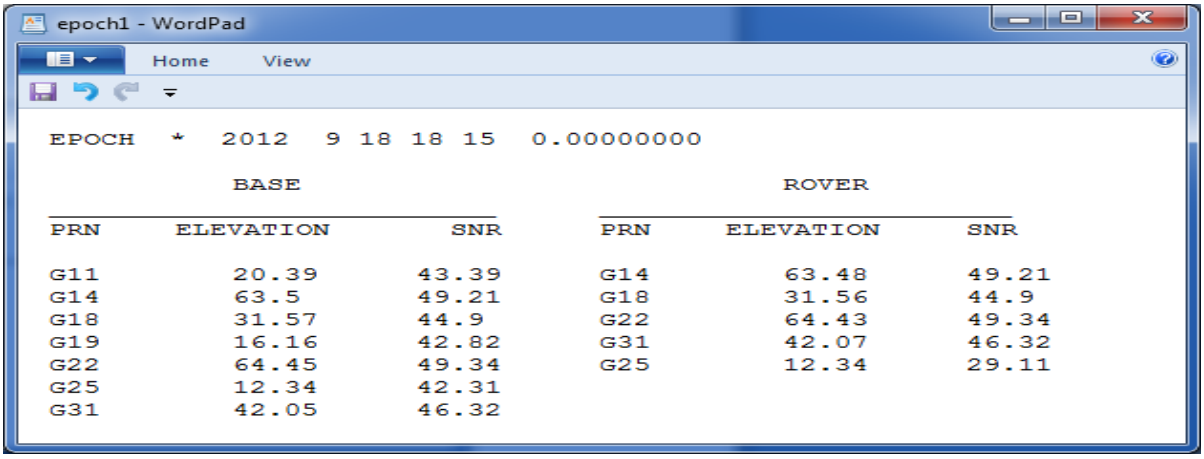

Figure 1.2 Output showing satellites visible at base and rover

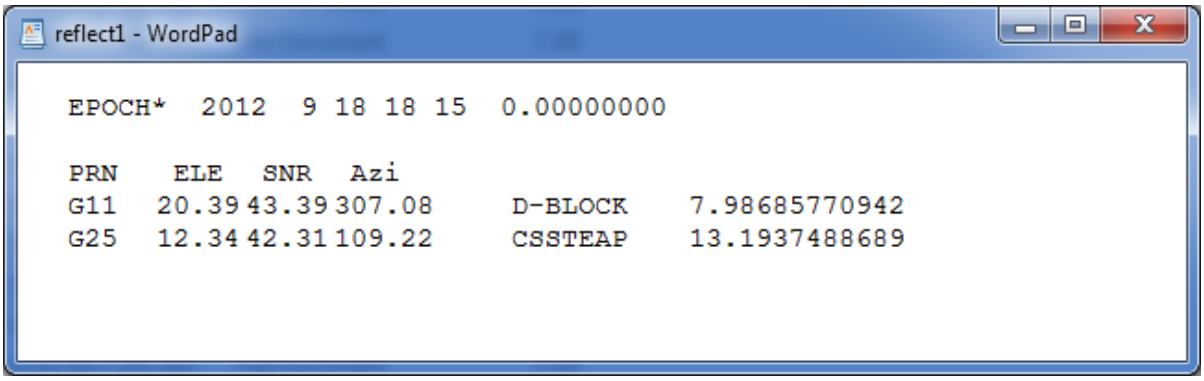

Figure 1.3 Reflected Satellites from buildings

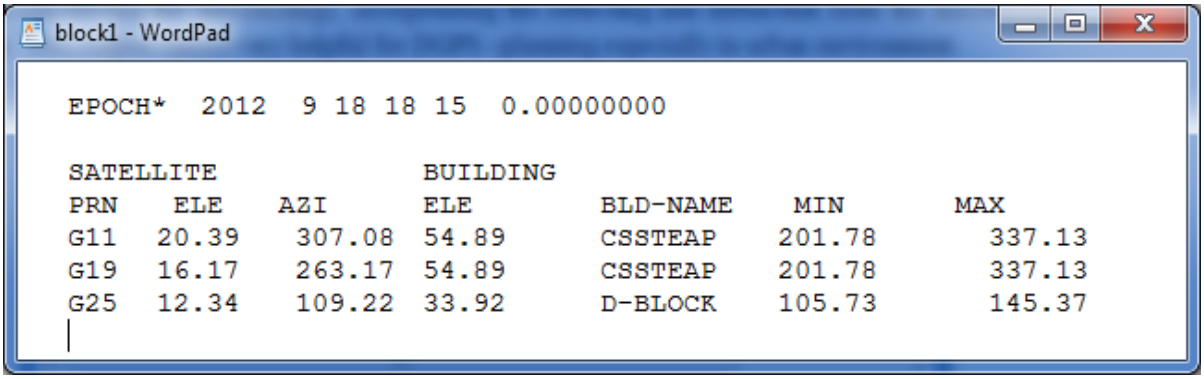

Figure 1.4 Blocked Satellites from buildings

The second folder contained the reflected satellites their elevation angle, azimuth angle with the mention of the buildings with which each PRN got reflected as shown in Figure 1.3. Third folder finally contained the blocked satellites and the buildings blocking them with their relative elevation and azimuth angle from the base, as shown in Figure 1.4.

Rinexe

The first menu bar button in this software is named Rinexe which has Open, Process, Save, About and Exit as submenus, shown in Figure 1.5. The sole purpose of this function is to extract the observables from RINEX 2.10 format to a MS Excel file. Open is used for entering the RINEX file to be processed. Process is used for extracting the observables from RINEX to MS Excel. Save, About and Exit perform functions as per there name imply. The output generated is a MS Excel file shown in Figure 1.6. Each sheet contains PRN no, Start time and end time of its acquisition. All the observables ranging from pseudorange to SNR are extracted along with their EPOCHS. This data is much need for further modeling of the multipath or extracting the residuals. This data is further used to analyze the relation between the SNR and multipath, at different antenna heights and with different building materials. The file is created with the same name as that of the rinex entered and saved in the same directory of the software in the folder named outputs.

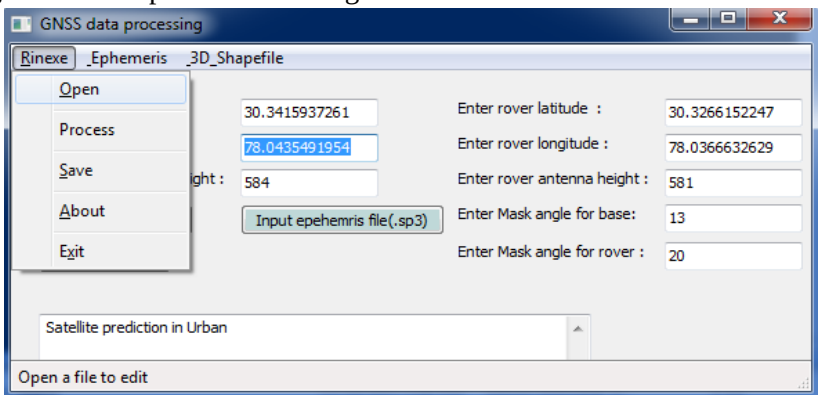

Figure 1.5 Rinexe submenu

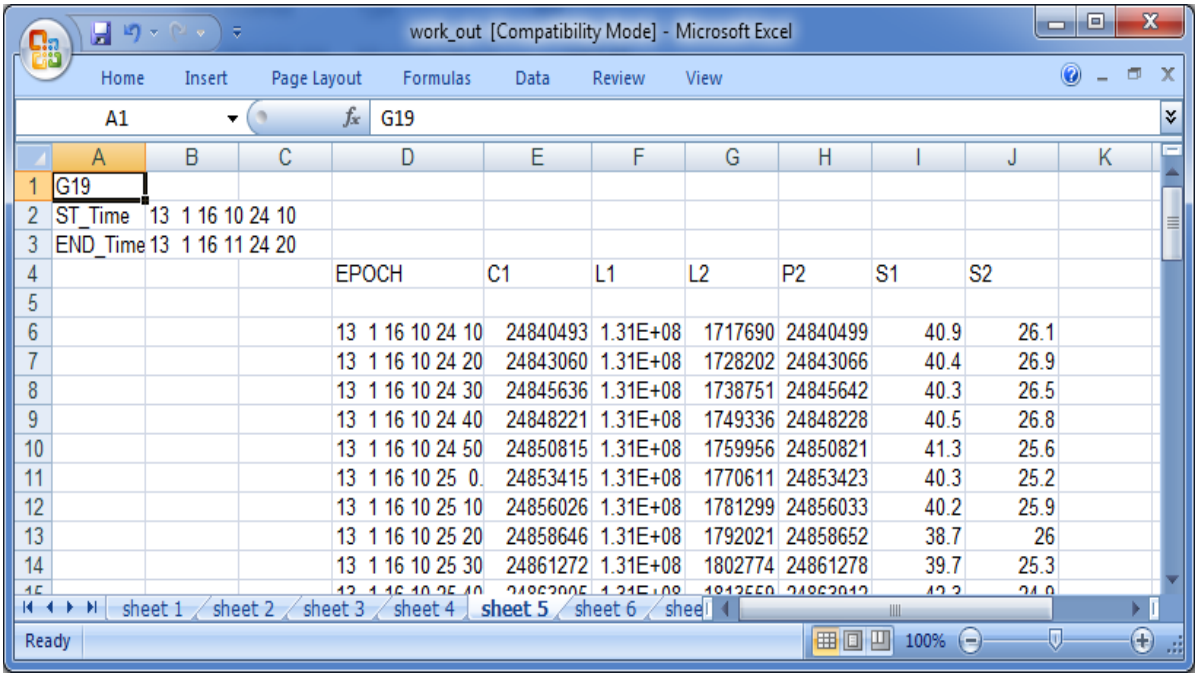

Figure 1.6 Output of Rinexe processing, observables stored in MS Excel

Ephemeris

The second menu bar button is the Ephemeris containing a number of submenus. The main objective of this part is to have graphical analysis especially for DGPS planning (with which a user can analyze the scenario of the satellites before going to field for DGPS surveying). The submenus are Visible Satellites, GDOP, Common Satellites, Sky Plot, Visibility and Satellite Visibility, which are shown in Figure 1.7. The location of the base and rover are entered in the main frame only, for which these graphs needs to be generated. The individual graphs can be saved as per the requirement.

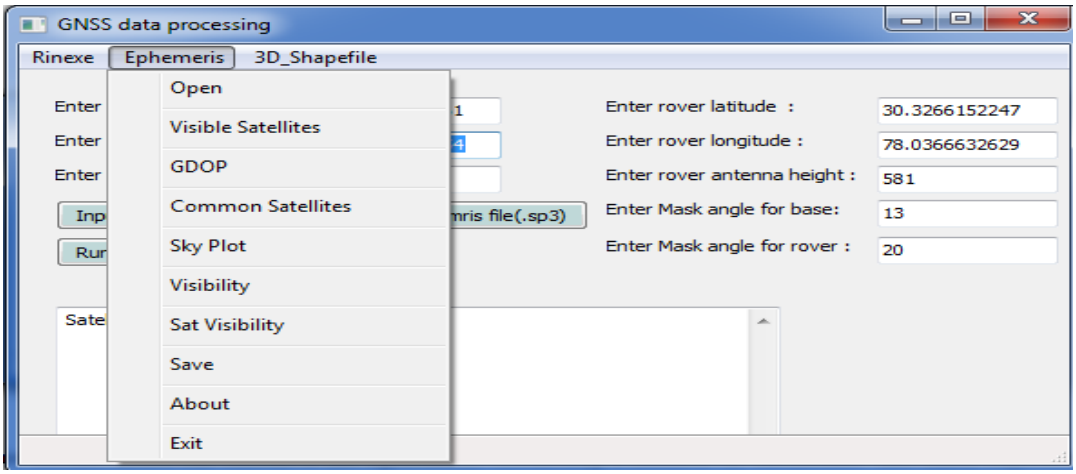

Figure 1.7 Ephemeris submenu

Visible Satellites

Once the Ephemeris file in .sp3 file is entered for which the prediction of satellites is to be done. The button is clicked for getting the number of satellites visible at all the epochs. This graph is a very helpful tool in GPS planning, as shown in Figure 1.8.

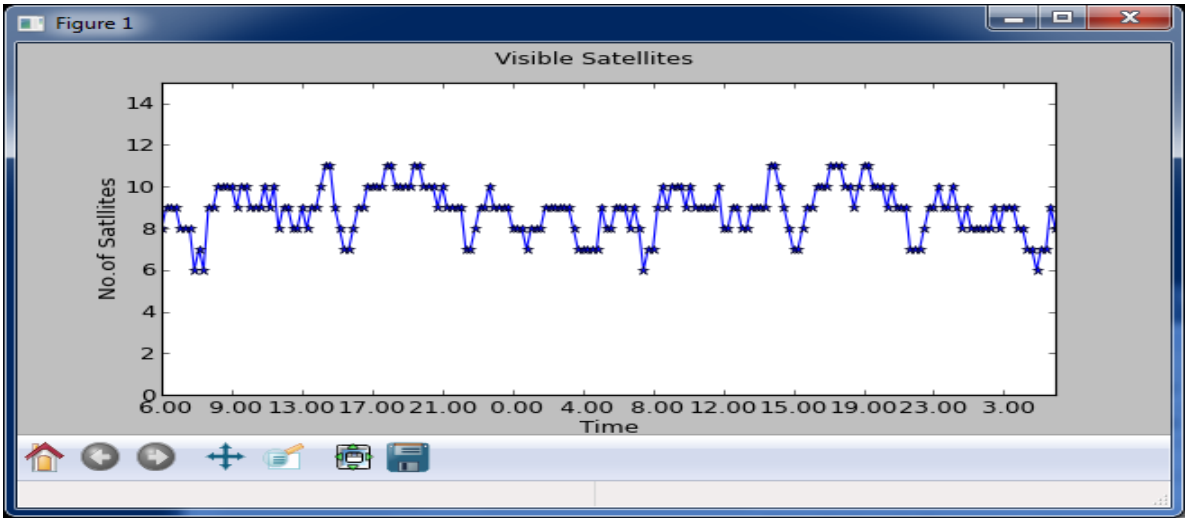

Figure 1.8 Number of Visible Satellites

GDOP

The GDOP values of the co-ordinates given in the base are mapped against the time, shown in Figure 1.9. The significance of the GDOP value is discussed in previous sections. This again is an important tool in GPS planning as it relates to the satellite geometry.

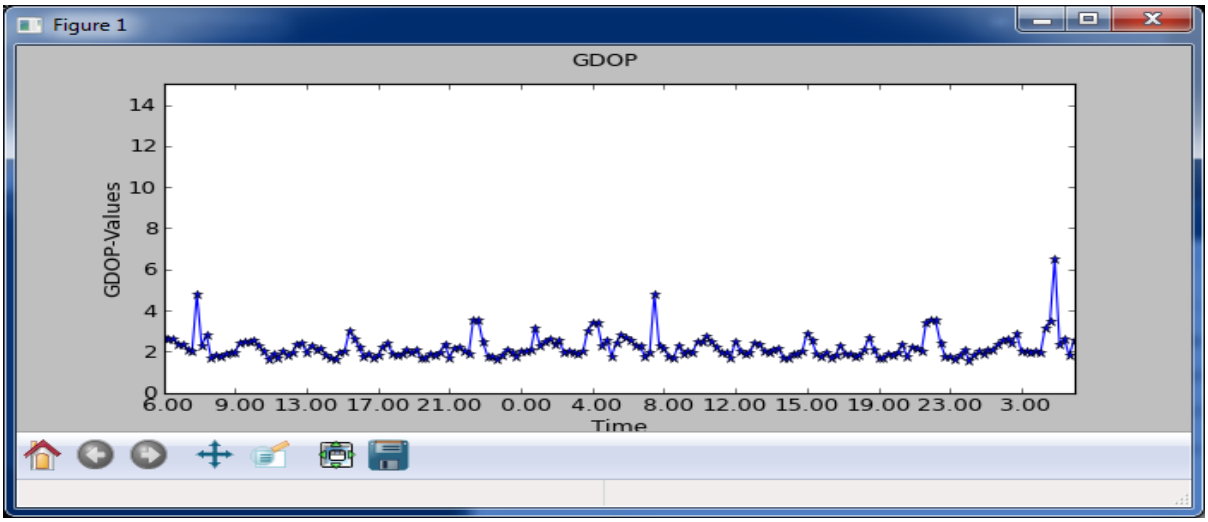

Figure 1.9 GDOP value

Common Satellites

This graph shows the common satellites of the base and rover of the co-ordinates given, for open environment is mapped against time, as shown in Figure 1.10.

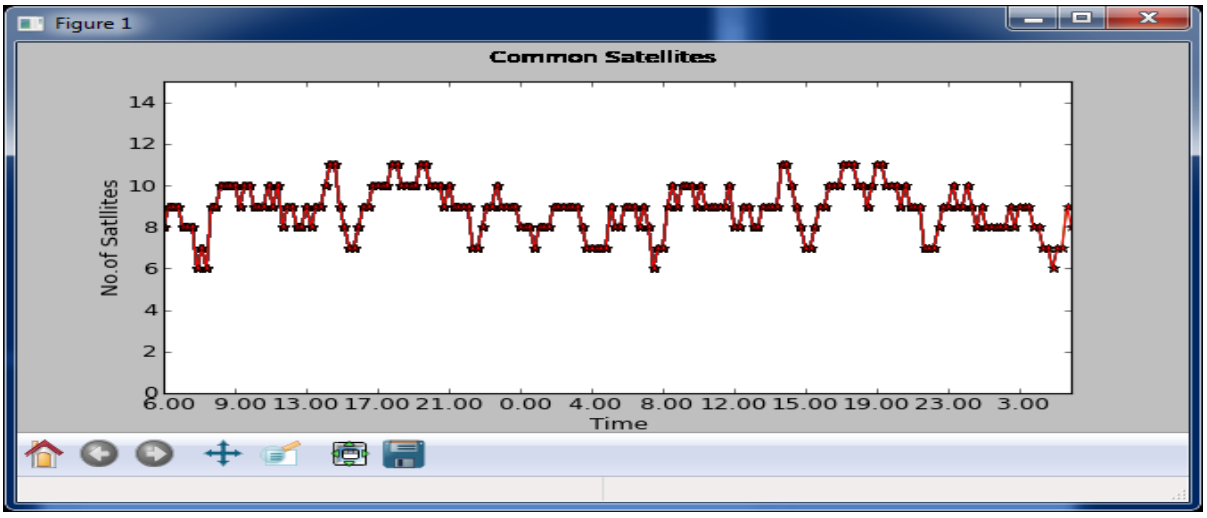

Figure 1.10 Common Satellites

Sky Plot

The sky plot represents the path of the satellite which it will take with respect to the GPS receiver whose co-ordinates are given in base text box. It combines the elevation and azimuth angle to map the

sky plot giving a fairly good idea to the user about the path a particular satellite would follow, as shown in Figure 1.11.

Visibility

The Figure 1.12 represents the visibility (elevation angle variation) of a particular satellite with respect to the time.

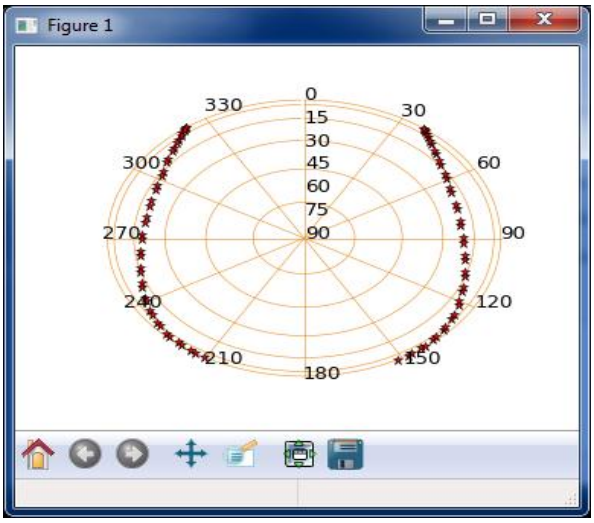

Figure 1.11 Sky plot of PRN 01

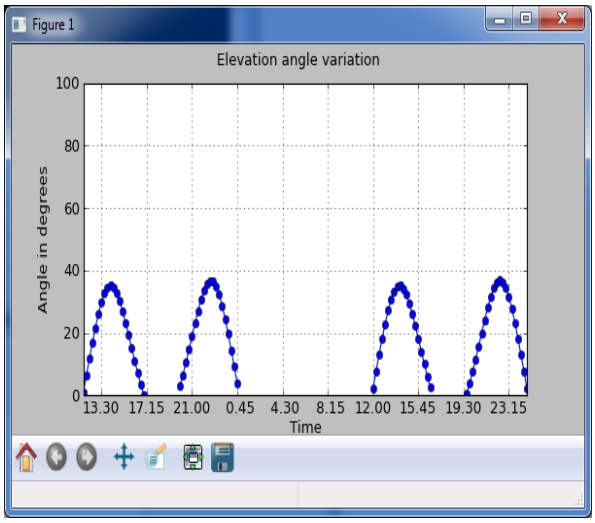

Figure 1.12 Elevation angle variation of PRN 01

Satellite Visibility Duration

This graph presents the duration of a particular satellite is visible over the location with base coordinates given, as shown in following Figure 1.13.

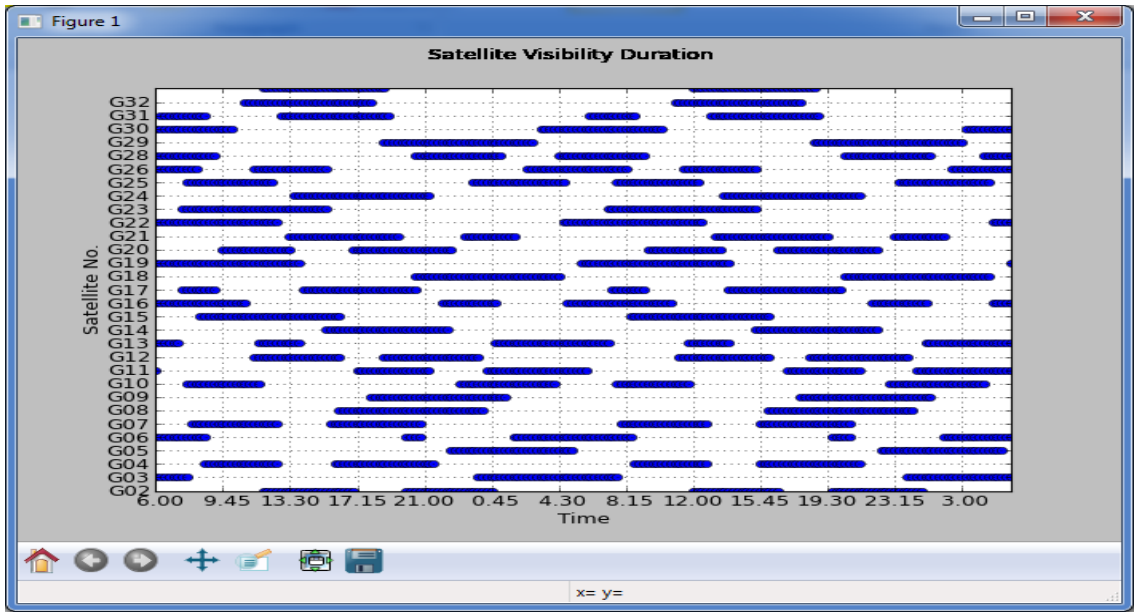

Figure 1.13 Satellite visibility duration of all the satellites

3D_Shapefile

The third menu is of 3D_Shapefile, which is developed for creating the 3D shapefile by entering the heights in the 2D building shapefile. From Cartosat DEM the corresponding ASCII File is generated containing the height with the co-ordinates. The menu is shown in Figure 1.14. This ASCII file along with the shapefile containing 2D-building footprints is entered and then the software gets all the points searched, if any point is lying inside the polygon; the height of the points found inside the building are as taken height of the building.

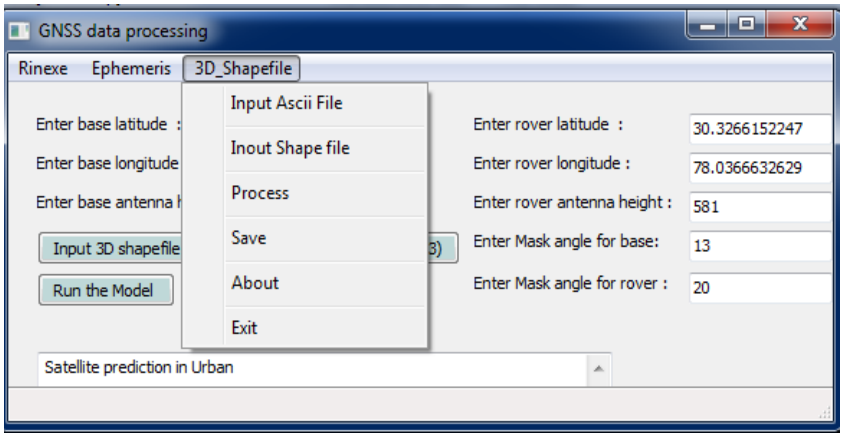

Figure 1.14 3D_Shapefile menu

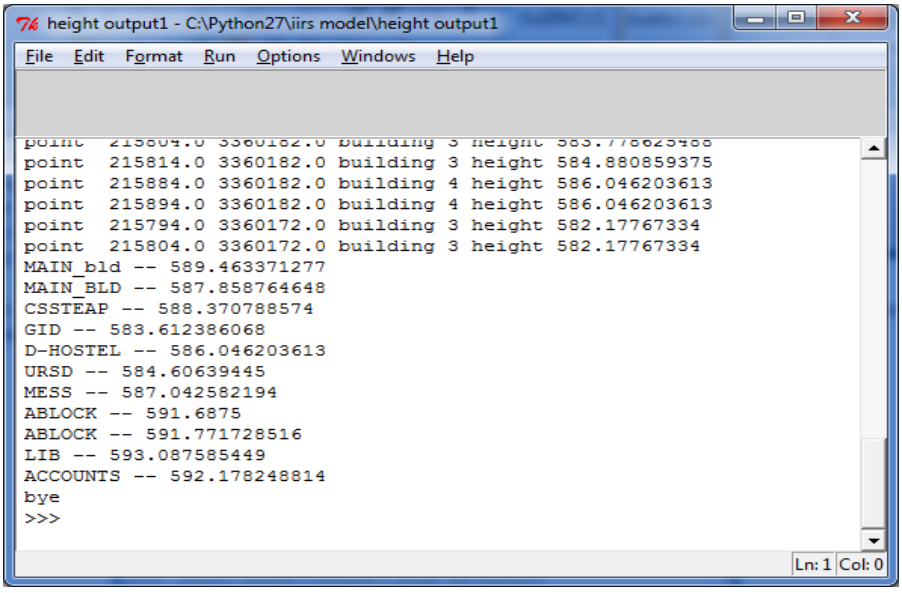

Figure 1.15 Output giving the building heights taken from Cartosat DEM

Figure 1.15 shows the output, which gives the heights along with the point coordinates lying on the building footprint.